Ablation of Cbl-b and c-Cbl in macrophages causes severe spontaneous lung inflammation via enhancing the M-CSFR signaling pathway

Jinping Zhang

j_pzhang@suda.edu.cn

Soochow University https://orcid.org/0000-0001-5537-5131

Fei Xu

Soochow University

Chensheng Tan

Soochow University

Kun Tang

Soochow University

Guodong Qiao

Soochow University

Yu Shao

Soochow University

Xiaoping Li

Soochow University

Ji Zhou

Soochow University https://orcid.org/0000-0002-5365-5751

Peijie Zhu

Soochow University

Mengyun Wu

Soochow University

Zhengrong Chen

Children's Hospital of Soochow University

Xiu Gao

Soochow University

Yufeng Wang

Children's Hospital of Soochow University

Beibei Huang

Soochow University

Yi Yang

Soochow University https://orcid.org/0000-0003-1620-1125

Chuangli Hao

Children's hospital of soochow university https://orcid.org/0000-0002-8203-0603

Article

Keywords:

Posted Date: December 4th, 2024

DOI: https://doi.org/10.21203/rs.3.rs-5497778/v1

Additional Declarations: There is **NO** Competing Interest.

Abstract

The Casitas B-lineage lymphoma (Cbl) family proteins are E3 ubiquitin ligases implicated in the regulation of various immune cells. However, their function in macrophages remains unclear. We show that macrophage-specific deficiency of Cbl-b and c-Cbl (Cbls) causes mice to die prematurely from spontaneous macrophage massive invasive lung inflammation. Mechanically, we identify that Cbls functions upstream of AKT and Erk to mediate the ubiquitination and degradation of M-CSFR. upon M-CSF stimulation, M-CSF binds to M-CSFR to activates downstream PI3K-AKT and Erk signaling pathways. At the same time, autophosphorylation of tyrosine at position 559 on M-CSFR receptor can promote receptor recruitment and phosphorylation of Cbls, and phosphorylated activated Cbls can target lysine at position 791 of M-CSFR for K63 linked-polyubiquitination modification. Eventually, the receptor is internalized and degraded through the lysosomal pathway, preventing the signaling pathway from being over-activated. Thus, Cbls deficiency in macrophages promotes M-CSF-induced activation of M-CSFR, AKT and Erk, which causes the accumulation of systemic macrophages due to increased cell proliferation and decreased apoptosis. Together, these data demonstrate that Cbl-b and c-Cbl play critical roles in the regulation of macrophage homeostasis by inhibiting M-CSFR-mediated AKT and Erk activation.

Introdution

Macrophages are an important part of the immune system, playing key roles in the primary response to pathogens and in coordinating adaptive immune responses, inflammation resolution, tissue homeostasis and repair [1]. In addition, the total number of macrophages has also been shown to be critical for the regulation of the immune system [2–7]. Thus, to ensure the proper function of immune system, the homeostasis, maturation, and total number of macrophages must be tightly regulated. Currently, there remain large gaps in our understanding of the mechanisms underlying the regulation of these processes in macrophages.

Macrophage colony-stimulating factor (M-CSF, also known as CSF-1) is essential for proliferation, survival, and differentiation of macrophages and their precursors [8–10]. M-CSF$^{op/op}$ mice develop osteoporosis due to lack of osteoclasts and defects in tissue macrophages and blood monocytes[11]. M-CSF binds to the M-CSF receptor (M-CSFR, also known as CSF-1R or CD115) and activates multiple downstream signaling events [10, 12, 13]. Specifically, the PI3K-AKT and Erk signaling pathways are critical for proliferation and survival of macrophages and their precursors [14–16].

Casitas B-Lymphoma (Cbl) is a family of E3 ubiquitin ligases containing ring finger. In mammals, the Cbl protein family contains of three members: Cbl-b, c-Cbl, and Cbl-3 [17–20], which play key negative regulatory roles in various signaling pathways [21–25]. Systemic double knockout of Cbls resulted in early fetal death in mice, while Cbl-b single knockout and c-Cbl single knockout did not affect birth and lifespan in mice, suggesting that Cbl-b and c-Cbl have important redundant functions in some biological

processes. Cbls plays important roles in the prevention of T-cell and B-cell-mediated autoimmune diseases [26, 27]. They regulate T and B cell development, tolerance, and function by regulating signals transmitted by T and B cell antigen receptors and coreceptors [22, 24]. In addition, studies have also found that mice specifically knocked out by DC cells of Cbl-b and c-Cbl developed severe spontaneous cirrhosis and liver fibrosis [28, 29]. The role of Cbls in macrophage biology, as compared to T, B and DC cells, and how members of the Cbl family cooperate in macrophages is currently unclear.

Here we found mice with deficiency in Cbl-b and c-Cbl in macrophages spontaneously developed severe lung inflammation disease with extensive macrophage infiltration. Moreover, we found that cellular proliferation of double knockout (dKO) macrophages were increased while cell apoptosis was decreased. Mechanistically, we report that both Cbl-b and c-Cbl are regulators of macrophage proliferation, apoptosis and M-CSF signaling by ubiquitinating and degradating M-CSFR, thereby inhibiting AKT and Erk activation. Studies have demonstrated that binding of M-CSF to CSF-1R activates PI3K and Erk signaling to promote macrophage proliferation and survival [14, 15, 30, 31]. We found that deficiency of Cbl-b and c-Cbl significantly upregulates M-CSFR protein levels, resulting in prolonged activation of AKT and Erk. Taken together, our data suggest that Cbl-b and c-Cbl exhibit functional redundancy in macrophage homeostasis and maturation.

Results

Cbl-b and c-Cbl-deficient mice develop severe lung disease

To investigate whether and how Cbl-b and c-Cbl cooperate in macrophages, we crossed Cbl-b$^{-/-}$ mice with Lyz2-Cre^{+} c-Cbl$^{flox/flox}$ mice to finally obtain four groups of mice: Lyz2-Cre^{-} c-Cbl$^{flox/flox}$ Cbl-b$^{+/+}$ (WT, thereafter), Lyz2-Cre^{-} c-Cbl$^{flox/flox}$ Cbl-b$^{-/-}$ (Cbl-b KO, thereafter), Lyz2-Cre^{+} c-Cbl$^{flox/flox}$ Cbl-b$^{+/+}$ (c-Cbl cKO, thereafter) and Lyz2-Cre^{+} c-Cbl$^{flox/flox}$ Cbl-b$^{-/-}$ (dKO, thereafter) mice (Fig. 1A). Deletion of c-Cbl mediated by Lyz2-Cre occurs predominantly in myeloid cells (including macrophages), and deletion of Cbl-b and c-Cbl in BMDMs was confirmed at protein level by Western blot (Fig. 1B). Figure 1A and Fig. 1B together confirmed the successful generation of Cbl-b KO, c-Cbl cKO and dKO mice.

During our study of Cbl-b KO, c-Cbl cKO, and dKO mice, we noticed that dKO mice died prematurely. DKO mice were born at normal Mendelian frequency (Supplementary Fig. 1A); however, within 2 weeks they became obviously sick, growth retarded, and most died within 2 months, with a maximum survival of no more than 3 months (Fig. 1C-E). By contrast, Cbl-b KO and c-Cbl cKO mice remained relatively healthy after birth. To explore the reason for the premature death of dKO mice, organs including hearts, livers, spleens, lungs and kidneys were dissected and examined. On morphologic examination, we observed that the lungs of dKO mice were significantly enlarged in appearance compared with other three groups of mice (Fig. 1F). Next, we found that the lungs of dKO pups at about 2 weeks of age already spontaneously developed serious lesions. Histologic analysis revealed that the number of alveoli in the lungs of dKO pups significantly decreased, the cells around the alveolar wall significantly increased, and

the alveolar wall significantly thickened (Fig. 1G). With the gradual development and maturity of dKO mice, the degree of lung lesions increased. At 6–8 weeks, the lung structure of dKO mice had been seriously damaged, and the existence of alveoli was almost invisible, and there were a large number of cells in the entire field of vision (Fig. 1G). And we observed no major abnormalities in hematoxylin and eosin (H&E) stained sections of dKO mice hearts, spleens, kidneys and livers (Supplementary Fig. 1B). Given the early and rapid development of lung lesions in dKO mice, this could be the main cause of premature deaths in dKO mice.

DKO macrophages accumulate in large numbers in lung, liver and spleen

Since only dKO mice developed severe lung disease, we speculated that some aspects of dKO macrophages might be altered relative to other three groups of macrophages, which enabled dKO macrophages to drive lung impaired directly or indirectly. To verify this, we analyzed macrophage compartments in lung. Compared with WT mice, total cell numbers in bronchoalveolar lavages fluid (BALF) were increased by 20-30-fold in dKO mice (data not shown). And we found the percentage and absolute number of alveolar macrophages (AMs) were significantly elevated in dKO BALF (Fig. 2A-C).

Lyz2-Cre transgenic mice are myeloid cell specific knockout tool mice, which are currently widely used for specific knockout of target genes in macrophages [32–34]. However, Lyz2-Cre is not a macrophage-specific marker. In addition to macrophages, Lyz2-Cre promoter is also active in several other myeloid cells, such as Monocytes, Neutrophils, and Dendritic cells (DCs), etc. The Western blot analysis results also showed that the double deletion of Cbl-b and c-Cbl occurred not only in macrophages, but also in other myeloid cells, while the deletion of Cbl-b only occurred in T and B Cells, and the expression of c-Cbl was normal (Fig. 2D).

Lung is known to contain various myeloid lineage cells such as AMs, interstitial macrophages (IMs), neutrophils, eosinophils, $CD11b^+$ DCs, $CD103^+$ DCs and monocytes. Therefore, it is also necessary to determine whether the proportion and absolute number of other myeloid immune cells in the lungs of dKO mice are affected by the double knockout of Cbl-b and c-Cbl. The results showed that the proportion and absolute number of AMs and IMs in the lungs of dKO mice increased significantly (Fig. 2E-J), while the proportion of $CD11b^+$ cDCs, $CD103^+$ cDCs and monocytes decreased significantly but the absolute number did not change significantly (Supplementary Fig. 2A-H). In addition, the proportion and absolute number of neutrophils and eosinophils in the lungs were significantly reduced (Supplementary Fig. 3A-F). In addition, Lyz2-Cre can also label type □ alveolar (AT2) cells [35], so we examined the proportion of AT2 cells and immune cells in the lungs of WT and dKO mice. The results showed that $CD45^+$ immune cells were mainly increased in the lungs of dKO mice, but not AT2 cells (Supplementary Fig. 4), and AMs were mainly increased in these immune cells. Together, these results indicated that macrophages subsets accumulate in the lungs of dKO mice and promote lung enlargement in dKO mice.

Inspection of other organs including spleen (Supplementary Fig. 5A-C) and liver (Supplementary Fig. 5D-F) revealed the same dominant accumulation of macrophages, indicating Cbl-b and c-Cbl affected the homeostasis of systemic macrophages.

Hyper-proliferation and impaired apoptosis of dKO macrophages contribute to the accumulation of macrophages in mice

The increased number of macrophages might be due to more efficient proliferation and/or less cell death. To investigate the reasons for dKO macrophages accumulation, we first analyzed cell proliferation and apoptosis. As expected, proliferating alveolar macrophages in the lungs of dKO mice was significantly increased and apoptotic AMs in the lungs of dKO mice was much decreased compared with other three groups of mice (Fig. 3A-C). Thus, these data indicated that deficiencies of Cbl-b and c-Cbl could promote macrophages proliferation and inhibit macrophages apoptosis, which could contribute to cell accumulation.

The proliferation and differentiation of macrophages depend on the interaction of their specific growth factors with receptors, namely M-CSF and its specific receptor M-CSFR. This interaction triggers cascade signalling pathways that promote differentiation, proliferation, survival, and normal function of macrophages [36–38]. The absence of ligands or receptors either impures the proliferation of macrophage populations or affects their differentiation [39–44]. To investigate whether the M-CSF/M-CSFR signaling pathway is involved in the proliferation and apoptosis of macrophages in dKO mice, we analyzed the proliferation and apoptosis of macrophages in M-CSF-dependent bone marrow (BM) cell culture system. First, we examined the proliferation capacity of BM cells with double knockout of Cbl-b and c-Cbl in M-CSF culture. In experiments, M-CSF is commonly used to induce macrophages from BM precursor cells. When cultured BM cells from four groups of mice with M-CSF, we found that the dKO BM cells produced more, larger, and denser macrophage clones under M-CSF stimulation compared to the control groups (Fig. 3D), and the total number of macrophages obtained by differentiation of dKO BM cells with M-CSF also increased significantly (Fig. 3E). Consistent with in vivo results, the proportion of $BrdU^+$ proliferating cells in dKO BMDMs was significantly increased compared to the control groups (Fig. 3F, G), confirming the hyperproliferative response to M-CSF of Cbl-b and c-Cbl-deficient cells. To verify the role of Cbl-b and c-Cbl in cell cycle progression, we measured the expression levels of mRNA transcripts encoding cell cycle-regulatory proteins in WT and dKO BMDMs cultured with M-CSF for 3 and 7 days. dKO BMDMs expressed more c-Myc, Cyclin D1and Cyclin D2 mRNA at day 3 and 7 compared with WT BMDMs (Fig. 3H). These data suggest that the absence of Cbl-b and c-Cbl promotes M-CSF-induced macrophage proliferation.

We also evaluated whether the effects of deficiencies of Cbl-b and c-Cbl on macrophage apoptosis were dependent on the presence of M-CSF. WT, Cbl-b KO, c-Cbl cKO and dKO BMDMs were cultured in the presence of M-CSF for 5 days, and then switched to M-CSF-free medium for 2 more days. After M-CSF deprivation, there was no significant change in apoptosis percentage of dKO BMDMs compared with the

control groups, nevertheless dKO BMDMs displayed a decreased percentage of apoptosis in the presence of M-CSF (Fig. 3I-L). These data suggest that the absence of Cbl-b and c-Cbl contributes to M-CSF-induced macrophage survival. Collectively, our findings demonstrate that Cbls negatively regulate M-CSF-induced macrophage proliferation and promoted macrophage apoptosis.

Meanwhile, we also analyzed cell development. We found that the percentages and absolute numbers of macrophage precursors/progenitors, including common myeloid progenitor (CMP) and granulocyte-macrophage progenitor (GMP), did not change among four groups of mice (Supplementary Fig. 6A-E), indicating that deficiencies of Cbl-b and c-Cbl did not affect macrophage development.

Both dKO AMs and BMDMs contribute to lung disease and injury

To explore whether dKO AMs could directly drive lung disease and injury, we conducted an adaptive transfer of BALF AMs purified from WT or dKO mice into WT recipient mice, respectively. Histologic analysis revealed that structural damage to the lungs of WT mice during adoptive transfer of AMs from dKO mice (Fig. 4A-B). These data suggested that dKO AMs could directly contribute to lung disease and injury.

In order to further explore whether dKO BMDMs could play a similar role to dKO AMs in lung injury, we conducted an adaptive transfer of BMDMs induced from bone marrow cells in WT or dKO mice into WT receptor mice, respectively. Histological analysis revealed that structural damage to the lungs of WT mice during adoptive transfer of BMDMs from dKO mice (Fig. 4C-D). These data suggested that, like dKO AMs, dKO BMDMs could also directly contribute to lung disease and injury.

dKO BMDMs exhibit prolonged AKT and Erk activation upon M-CSF stimulation

The excessive proliferation and improved survival of M-CSF-induced dKO macrophages suggests that Cbls are involved in the regulation of M-CSF signalling. Studies have shown that binding of M-CSF to M-CSFR activates PI3K-AKT and Erk signalling to promote macrophage proliferation and survival. We therefore examined whether deficiencies of Cbl-b and c-Cbl enhanced PI3K-AKT and Erk signalling. Since we could not obtain enough pulmonary macrophages for a biochemical study, we used BM cell derived macrophages in our experiments. We attempted to stimulate WT, Cbl-b KO, c-Cbl cKO and dKO BMDMs with M-CSF at different time points and analysed the activation of these signalling pathways by Western blot. The results showed that activated p-AKT was barely detectable in unstimulated WT, Cbl-b KO and c-Cbl cKO BMDMs, whereas M-CSF stimulation significantly increased AKT activity for a short period of time, but rapidly decreased AKT activity to the lowest level with prolonged stimulation (Fig. 5A-C). However, during M-CSF stimulation, AKT in dKO BMDMs remained in a state of continuous phosphorylation (Fig. 5A-C). After 30 minutes of stimulation with M-CSF, p-AKT decreased to a very low level in WT, Cbl-b KO, c-Cbl cKO and dKO BMDMs, but after 6 hours of stimulation with M-CSF, a high

expression level of p-AKT could still be detected in dKO BMDMs (Fig. 5A-C). In contrast, Erk activation did not seem to be significantly affected by Cbls deficiency (Fig. 5A-C). However, we found that after 30 minutes of stimulation with M-CSF, the expression level of p-Erk was relatively higher in dKO BMDMs than in the control group (Fig. 5A-C). We suspected that the change in Erk activity might occur in the early period, so we controlled the stimulation time of M-CSF within 30 minutes, and then analysed the activation of Erk by Western blot. The results showed that although p-Erk in WT, Cbl-b KO, c-Cbl cKO and dKO BMDMs had decreased to a lower level within 20–30 minutes of stimulation with M-CSF, the expression level of p-Erk in dKO BMDMs was still higher than that of the control group (Fig. 5D-F). These results indicated that the double knockout of Cbl-b and c-Cbl significantly prolonged the activation of AKT and Erk stimulated by M-CSF. Taken together, these findings suggest that Cbl-b and c-Cbl may be involved in macrophage proliferation by regulating the M-CSF/M-CSFR signalling pathway.

In order to further explore the molecular mechanism of Cbls involved in macrophage apoptosis by regulating M-CSF/M-CSFR signalling pathway. We detected the expression levels of apoptosis-related proteins in WT and dKO BMDMs induced with M-CSF by Western blot. It is well known that the Caspase family plays a crucial role in the process of apoptosis, and Cleaved Caspase-3 and Cleaved Caspase-7 are the key executive molecules [45, 46]. The above flow detection results showed that in the presence of M-CSF, the proportion of apoptotic cells in dKO BMDMs was significantly reduced compared with WT BMDMs (Fig. 3K, L). We further confirmed this result by using Western blot to measure the cleavage of effector caspases downstream of apoptosis pathway, including caspase-3 and caspase-7. Consistently, the cleavage of caspase-3, caspase-7 and caspase-9 were much lower in dKO BMDMs, with no change for intact forms (Supplementary Fig. 7). In addition, the protein expression levels of pro-apoptotic molecule Bim in dKO BMDMs were significantly decreased, while the protein expression levels of the anti-apoptotic molecule Bcl-xL were significantly increased (Supplementary Fig. 7). Taken together, these findings suggest that Cbl-b and c-Cbl may be involved in macrophage apoptosis by regulating the M-CSF/M-CSFR signalling pathway.

Cbl-b and c-Cbl collaboratively inhibit M-CSF-dependent cell proliferation and promote cell apoptosis by down-regulating M-CSFR protein levels

Since the function of M-CSF is mediated by its specific receptor M-CSFR, we hypothesized that Cbl-b and c-Cbl may play a role in regulating M-CSF/M-CSFR signaling by influencing M-CSFR expression. To further confirm the regulatory relationship between Cbls and M-CSF/M-CSFR signalling pathway. We examined M-CSFR expression on the surface of AMs from WT, Cbl-b KO, c-Cbl cKO and dKO mice. Flow cytometric analysis revealed that M-CSFR expression was significantly higher on dKO AMs compared to that on WT, Cbl-b KO and c-Cbl cKO AMs (Fig. 6A). However, qPCR results showed that the double knockout of Cbl-b and c-Cbl did not affect the expression of M-CSFR mRNA (Fig. 6B). Consistent with the results in vivo, we found that M-CSFR protein levels were significantly increased in dKO BMDMs compared with those in other three counterparts (Fig. 6C), indicating Cbl-b and c-Cbl collaborated to down-regulated M-CSFR protein levels.

To verify the positive role of M-CSFR on macrophage proliferation in dKO mice, specific inhibitor BLZ945 for M-CSFR was added into the culture system used for induction of BMDMs, and then cell proliferation was assessed by flow cytometry. Results showed the addition of BLZ945 significantly inhibited the formation of macrophage clones in dKO mice (Fig. 6D) and significantly decreased the percentage of proliferating dKO BMDMs (Fig. 6E, F). Next, M-CSF was used to stimulate dKO BMDMs at different time points and BLZ945 was combined to treat the cells. Finally, Western blot was used to analyze the activation of M-CSF/M-CSFR downstream signaling pathway. The results showed that the levels of p-AKT and p-Erk in dKO BMDMs were significantly increased after M-CSF stimulation, whereas the phosphorylation of AKT and Erk induced by M-CSF stimulation was effectively reduced after BLZ945 treatment of dKO BMDMs (Fig. 6G), suggesting that M-CSFR indeed participated the proliferation of macropahges controlled by Cbl-b and c-Cbl.

To further verify the negative role of M-CSFR on macrophage proliferation in dKO mice, specific inhibitor BLZ945 for M-CSFR was added into the culture system used for induction of BMDMs, and then cell apoptosis was assessed by flow cytometry. Results showed the addition of BLZ945 increased the percentage of apoptotic dKO BMDMs (Fig. 6H, I). Next, we treated dKO BMDMs with BLZ945, and then analyzed the expression levels of apoptosis-related proteins downstream of M-CSF/M-CSFR signaling pathway by Western blot. The results showed that the treatment of dKO BMDMs with BLZ945 resulted in protein expression levels of Cleaved caspase-3, Cleaved caspase-7, Cleaved caspase-9 and the pro-apoptotic molecule Bim were significantly increased, while protein expression levels of the anti-apoptotic molecule Bcl-xL were significantly decreased (Fig. 6J), suggesting that M-CSFR indeed participated the apoptosis of macrophages controlled by Cbl-b and c-Cbl.

Cbls mediate M-CSF-induced the ubiquitination and degradation of M-CSFR

As members of the Cbl family are E3 ubiquitin ligases, we next investigated whether Cbls negatively regulate M-CSFR via ubiquitination and degradation. Since endogenous M-CSFR was not expressed in HEK293T cells, we constructed an overexpression plasmid of M-CSFR and confirmed that M-CSFR could be expressed on the cell membrane of HEK293T cells by Western blot and flow cytometry (Supplementary Fig. 8A, B). First, we found that exogenous M-CSFR was associated with Cbl-b or c-Cbl when they were co-expressed in HEK293T cells (Fig. 7A, B). Furthermore, endogenous M-CSFR was inducibly associated with Cbl-b or c-Cbl in MH-S cells (Supplementary Fig. 8C, D). and BMDMs (Fig. 7C, D) after stimulation with M-CSF. To investigate whether Cbls could ubiquitinate and degrade M-CSFR, we co-expressed M-CSFR with Cbl-b or c-Cbl in HEK293T cells and examined the ubiquitination and degradation of M-CSFR with or without M-CSF stimulation. Overexpression of either Cbl-b or c-Cbl significantly promoted the ubiquitination and degradation of M-CSFR after stimulation with M-CSF (Fig. 7E, F). In contrast, overexpression of either Cbl-b C373A or c-Cbl C379A, two ubiquitin E3 ligase inactive mutants of Cbl-b and c-Cbl, significantly down-regulated M-CSFR ubiquitination and prevented M-CSFR degradation (Supplementary Fig. 8E-H). To further confirm the effect of endogenous Cbl-b and

c-Cbl in primary cells on the ubiquitination modification of M-CSFR, we stimulated BMDMs from WT and dKO mice with M-CSF. We found that M-CSF stimulation significantly enhanced M-CSFR ubiquitination in WT BMDMs (Fig. 7G). However, double deletion of Cbl-b and c-Cbl significantly reduced M-CSF-induced M-CSFR ubiquitination (Fig. 7G). Since the two molecules, Cbl-b and c-Cbl, co-exist in WT BMDMs, we wanted to further explore whether endogenous Cbl-b or c-Cbl can play the same role when they are present alone. Next, we stimulated BMDMs from WT, Cbl-b KO, c-Cbl KO and dKO mice with M-CSF. We found that compared with WT BMDMs, M-CSFR in Cbl-b KO and c-Cbl cKO BMDMs can still undergo significant polyubiquitination modification under M-CSF stimulation (Fig. 7H). However, M-CSFR in dKO mouse BMDMs did not undergo significant polyubiquitination modification under M-CSF stimulation (Fig. 7H). Consequently, the signal-induced degradation of M-CSFR after M-CSF stimulation was significantly blocked only in dKO BMDMs but not in Cbl-b-deficient or c-Cbl-deficient BMDMs (Fig. 7I-K).

To further understand the pathways by which Cbl-b and c-Cbl promote M-CSFR degradation, we treated HEK293T cells with either CQ (a lysosome inhibitor) or MG132 (a proteasome inhibitor). The results showed that lysosomal inhibition by CQ significantly blocked Cbl-b and c-Cbl-mediated M-CSFR degradation after M-CSF stimulation, whereas MG132 had no effect on proteasome inhibition (Fig. 7L). Thus, these data indicate that both Cbl-b and c-Cbl target M-CSFR for lysosomal degradation after M-CSF stimulation.

Phosphorylation of Cbls and autophosphorylation of M-CSFR are critical for M-CSFR ubiquitination and degradation

Studies have shown that both Cbl-b and c-Cbl contain various tyrosine residues, which can be phosphorylated under multiple stimuli, and tyrosine phosphorylation of Cbl-b and c-Cbl is critical for their biological activity [47, 48]. To further investigate whether Cbl-b and c-Cbl can undergo tyrosine phosphorylation during M-CSF stimulation, we stimulated MH-S cell line or WT mice primary BMDMs with or without M-CSF. We found that M-CSF stimulation can induce prominent tyrosine phosphorylation of both Cbl-b and c-Cbl (Fig. 8A-D). To determine whether the tyrosine phosphorylation of Cbls is mediated by their target kinase M-CSFR, we expressed Cbls alone or with M-CSFR in HEK293T cells, and then measured the tyrosine phosphorylation levels of Cbls with or without M-CSF stimulation. The results showed that M-CSF stimulation did not induce tyrosine phosphorylation when Cbl-b or c-Cbl was expressed alone, but M-CSF stimulation significantly increased the tyrosine phosphorylation level of Cbl-b or c-Cbl when they were co-expressed with M-CSFR (Fig. 8E, F). When M-CSFR loses its kinase activity, it cannot mediate tyrosine phosphorylation of Cbl-b or c-Cbl (Fig. 8G, H). These results suggest that M-CSFR can mediate tyrosine phosphorylation of Cbl-b or c-Cbl after M-CSF stimulation, depending on the presence of M-CSFR receptor tyrosine kinase activity.

Based on previous studies of Cbls and information from the UniProt database, we noticed that Cbl-b contains four of the most significantly phosphorylated tyrosine (Tyr, F) residues (including Tyr363, 664, 708 and 889) and c-Cbl contains five of the most significantly phosphorylated tyrosine residues (Tyr369,

672, 698, 737 and 780). To further investigate whether M-CSFR-mediated tyrosine phosphorylation of Cbls during M-CSF stimulation has an effect on ubiquitination and degradation of M-CSFR, we mutated each tyrosine (Y) residue to phenylalanine (F) to simulate non-phosphorylation. Overexpression of either Cbl-b Y363F or c-Cbl Y369F in HEK293T cells did not promote the degradation of M-CSFR during M-CSF stimulation (Fig. 8I, J). Furthermore, overexpression of either Cbl-b Y363F or c-Cbl Y369F in HEK293T cells significantly down-regulated the level of M-CSFR polyubiquitination modification during M-CSF stimulation (Fig. 8K, L). These results suggest that tyrosine phosphorylation of M-CSFR at Cbl-b Tyr-363 or c-Cbl Tyr-369 mediates ubiquitination and degradation of M-CSFR by Cbl-b or c-Cbl, respectively, during M-CSF stimulation.

We also found that when the kinase activity of M-CSFR was lost, Cbl-b and c-Cbl were unable to degrade the M-CSFR kinase inactivated mutant K614M during M-CSF stimulation (Supplementary Fig. 9A). Consistent with these results, overexpression of either Cbl-b or c-Cbl significantly up-regulated the polyubiquitination level of M-CSFR (WT) under M-CSF stimulation, whereas overexpression of either Cbl-b or c-Cbl did not up-regate the polyubiquitination level of M-CSFR kinase inactivated mutant K614M (Supplementary Fig. 9B, C). These results suggest that M-CSFR kinase activity is required for M-CSFR ubiquitination and degradation through Cbls.

M-CSF binds to M-CSFR on the cell surface to dimerize M-CSFR, and dimerization activates M-CSFR tyrosine autophosphorylation and recruitment of related signaling proteins. Since M-CSFR is autophosphorylated during M-CSF stimulation, we wondered what the impact of these events is on M-CSFR stability. First, we stimulated WT BMDMs with M-CSF at different time points, and treated the cells in combination with M-CSFR inhibitor BLZ945 (BLZ945 acts as a potent and selective small molecule inhibitor of M-CSFR receptor tyrosine kinase, blocking the autophosphorylation activation of M-CSFR), and then detected the protein expression level of M-CSFR. The results showed that M-CSFR in WT BMDMs was rapidly degraded during M-CSF stimulation, and the treatment of WT BMDMs with BLZ945 effectively prevented M-CSFR degradation induced by M-CSF stimulation (Supplementary Fig. 9D). These results suggest that BLZ945 inhibition of autophosphorylation activation of M-CSFR can effectively prevent the degradation of M-CSFR.

Based on previous studies of M-CSFR and information from the UniProt database, we noticed that M-CSFR contains eight of the most significantly phosphorylated tyrosine (Tyr, F) residues (including Tyr544, 559, 697, 706, 721, 807, 921 and 974). To examine whether autophosphorylation is required for M-CSFR ubiquitination and degradation by Cbl-b and c-Cbl, we each tyrosine (Y) residue to phenylalanine (F) to simulate non-phosphorylation and construct a series of M-CSFR phosphorylated mutant plasmids. We found that overexpression of either Cbl-b or c-Cbl effectively promoted the degradation of M-CSFR WT, Y544F, Y697F, Y706F, Y721F, Y807F, Y921F and Y974F after stimulation with M-CSF, but not Y559F (Supplementary Fig. 9E, F). Importantly, mutation of Tyr559 abolished Cbl-b or c-Cbl-mediated ubiquitination of M-CSFR induced by M-CSF stimulation (Supplementary Fig. 9G, H). These data suggest that autophosphorylation of Tyr559 is critical for M-CSFR ubiquitination and degradation by Cbls.

Cbls mediate the K63-linked polyubiquitination modification at Lys791 of M-CSFR

We further analysed the putative lysine (Lys, K) residues of M-CSFR with ubiquitination modifications from the Protein Lysine Modifications Database (PMLD). We noticed that there are six potential ubiquitinated lysine residues on M-CSFR including Lys572, 584, 604, 698, 791 and 868 (Fig. 9A). Next, we further used the NCBI database to perform site sequence homology comparison, and the results showed that K791 was a conserved ubiquitination motif in the M-CSFR homology (Fig. 9B). This suggested that K791 might be a site of polyubiquitination modification on M-CSFR. To verify this hypothesis, we mutated each lysines (K) residue to arginines (R). We found that overexpression of either Cbl-b or c-Cbl effectively promoted the degradation of M-CSFR WT, K572R, K584R, K604R, K698R and K868R after stimulation with M-CSF, but not K791R (Fig. 9C, D). Importantly, mutation of Lys791 abolished Cbl-b or c-Cbl-mediated ubiquitination of M-CSFR induced by M-CSF stimulation (Fig. 9E, F). These data suggest that Cbls induce polyubiquitination of M-CSFR at Lys791 during M-CSF stimulation.

To determine which type of polyubiquitin linkage to M-CSFR is catalysed by Cbls, we transfected M-CSFR and Cbl-b or c-Cbl into HEK293T cells together with different ubiquitin mutant types of HA-Ub, including K6, K11, K27, K29, K33, K48 and K63, each of which contains only one lysine available for polyubiquitination. We found that overexpression of either Cbl-b or c-Cbl significantly promoted K63-linked polyubiquitination of M-CSFR after stimulation with M-CSF (Fig. 9G, H). Furthermore, mutation of Lys791 largely inhibited Cbl-b or c-Cbl-mediated K63-linked polyubiquitination of M-CSFR after stimulation with M-CSF (Supplementary Fig. 10A, B). At the same time, we found that M-CSF stimulation significantly enhanced M-CSFR K63-linked polyubiquitination in WT BMDMs (Fig. 9I). However, double deletion of Cbl-b and c-Cbl significantly reduced M-CSF-induced M-CSFR K63-linked polyubiquitination (Fig. 9I). Thus, we demonstrated that Cbls induce K63-linked polyubiquitination at Lys791 of M-CSFR during M-CSF stimulation, leading to M-CSFR protein endogenous degradation via the lysosomal pathway.

Discussion

Tissue-resident macrophages provide immune defense and help establish and maintain tissue homeostasis. Studies have shown that in a stable state, tissue-resident macrophage AMs in the lung is required to clear dead cells and cell debris or release soluble mediators, thereby avoiding host damage and protecting lung function. The absence or dysfunction of AMs can lead to PAP [2–5]. Tissue-resident macrophage OCs in bone tissue are responsible for bone resorption and together with bone formation in OBs form homeostasis to maintain bone homeostasis. The decrease or dysfunction of OCs can lead to the decrease of bone resorption and the increase of cortical bone and calcified cartilage, leading to osteosclerosis [6, 7]. This indicates that the precise control of the stable number of macrophages in tissues and organs is very important for maintaining body health. In this study, we found that knocking out Cbls in macrophages altered the homeostasis of macrophage numbers, leading to a significant

increase in the number of macrophages in spleen, liver, and especially lung tissue. dKO mice exhibit spontaneous chronic lung inflammation. Therefore, our study shows that Cbls is a key regulator in maintaining tissue macrophage number homeostasis and demonstrates that altering the homeostasis of macrophage number disrupts the body's health state.

The balance of proliferation rate and apoptosis rate together stabilized the number of macrophages. Here, we found that simultaneous loss of c-Cbl and Cbl-b in macrophages leads to massive accumulation of macrophages in spleen, liver, and lung tissues by promoting proliferation and inhibiting apoptosis. Since there was no significant change in the proportion and absolute number of macrophages in either Cbl-b or c-Cbl single-knockout mice, this suggests that Cbl-b and c-Cbl have overlapping functions in regulating macrophage proliferation and apoptosis. The signaling pathway activated by M-CSF and its receptor M-CSFR can regulate the development of most tissue macrophages such as OCs and AMs, playing an important role in development and innate immunity [36]. Macrophages in many tissues of $Csf1^{op/op}$ and $M\text{-}CSFR^{-/-}$ mice are deficient, and they all suffer from severe osteosclerosis, which is caused by the loss of OCs leading to decreased bone resorption [39]. In addition to OCs, the lung tissue of young $Csf1^{op/op}$ mice was relatively deficient in AMs, which returned to normal in adulthood, and even then, adult $Csf1^{op/op}$ mice spontaneously developed emphysema [49]. These suggested that M-CSF may have a relatively greater importance in the perinatal and neonatal period than in adulthood. And M-CSF may be important for the normal AM function throughout life. Moreover, M-CSF and its receptor M-CSFR can trigger multiple cascade signaling pathways that promote differentiation, proliferation, survival and normal function of macrophages, such as PI3K-AKT and Erk signaling pathways [14, 15, 30, 31]. However, whether Cbl-b and c-Cbl can jointly regulate the M-CSF/M-CSFR signaling pathway to maintain the number and function of macrophages in the body has not been studied. In this study, we found that the simultaneous deletion of c-Cbl and Cbl-b in macrophages led to the sustained activation of AKT, the main target of PI3K downstream of the M-CSF/M-CSFR signaling pathway, which significantly promoted the proliferation of macrophages and inhibited their apoptosis, ultimately leading to a significant increase in the number of macrophages. Data from adoptive transfer experiments indicated that, like dKO AMs, M-CSF induced dKO BMDMs could also directly initiate or drive lung disease and injury. Moreover, as we all know, AT2-derived GM-CSF is crucial for both AM development and maintenance [50]. We also attempted to stimulate WT and dKO BMDMs with GM-CSF at different time points and analysed the activation of downstream signalling pathways by Western blot. The results showed that there was no significant difference in p-STAT5, p-AKT and p-Erk between WT and dKO BMDMs with the change of GM-CSF stimulation time (Supplementary Figure. 12). Therefore, based on the experimental results, we believe that the deletion of Cbl-b and c-Cbl may not greatly affect the transduction of CSF2R signaling pathway in our dKO mice model.

Although as early as 1999, it has been reported that c-Cbl can ubiquitinate M-CSFR to promote its internalization and degradation. However, the researchers found that although the M-CSF/M-CSFR complex on the surface of $c\text{-}Cbl^{-/-}$ macrophages was internalized more slowly, it still could not avoid the complete degradation of M-CSFR, suggesting that the absence of c-Cbl alone was not sufficient to

completely prevent the ubiquitination degradation of M-CSFR. This suggests that there are other factors besides c-Cbl that can regulate the degradation of M-CSFR [51]. Our study found that Cbls can negatively regulate the M-CSF/M-CSFR signaling pathway by promoting ubiquitination degradation of M-CSFR. Because Cbl-b and c-Cbl proteins are structurally similar and homologous, they can both perform the function of ubiquitination to degrade M-CSFR. In addition, we further clarified the specific ubiquitination sites and the types of polyubiquitination connections that Cbl-b and c-Cbl regulate M-CSFR.

In addition, our study showed that AMs in dKO mice were different from AMs in WT mice, with high expression of M2-type macrophage surface marker CD206 (Supplementary Fig. 11A, B), suggesting that AMs in dKO mice migrated to M2 phenotype, and Cbl-b and c-Cbl could inhibit macrophage migration to M2 phenotype in vivo. By detecting the expression of inflammatory factors in lung tissue, we also found that the expression levels of M2-related anti-inflammatory cytokines IL-4 and IL-10 were significantly increased, while the expression levels of M1-related pro-inflammatory cytokines, such as IL-1β, IL-12 and IFN-γ, were significantly decreased except for the expression levels of IL-6 (Supplementary Fig. 10C, D). It is suggested that a large number of AMs in the lung tissue of dKO mice may cause M2 phenotypic shift, causing chronic pulmonary inflammation. It has been reported that Src Homology 2-containing Inositol Phosphatase-1 (SHIP-1) can also inhibit the migration of macrophages to M2 phenotype in vivo. Macrophages in SHIP-1$^{-/-}$ mice also migrated to the M2 phenotype [52]. This is similar to the phenotype of our dKO mice. SHIP-1 can control the intracellular level of PI3K product PIP3 through dephosphorylation of PIP3 and is a negative regulator of the PI3K-AKT pathway [53, 54]. The main reason for M2 phenotypic shift of macrophages in mice induced by SHIP-1 knockout is the increase of intracellular PIP3 level in the critical stage of cell development. Then, like SHIP-1, the double knockdown of Cbl-b and c-Cbl can also cause the M-CSF/M-CSFR/PI3K/AKT signaling pathway to be continuously activated. Moreover, a large number of studies have reported that M-CSF can promote the polarization of M2-type macrophages [55–60]. For example, many tumor cells can highly express M-CSF, and M-CSFR acts on macrophages in the tumor microenvironment to differentiate into M2-type TAMs. TAMs, on the other hand, can inhibit the anti-tumor immune response by promoting the formation of tumor blood vessels and the proliferation of endothelial cells, and ultimately play a role in promoting the development and metastasis of tumors [61–63]. Not only is M-CSF overexpressed in tumors, but elevated M-CSFR levels are also associated with poor prognosis in patients with various cancers, and targeting M-CSFR signaling in tumor-promoting Tams is an attractive strategy for eliminating or repolarizing these cells [64–67]. Therefore, we have reason to believe that Cbl-b and c-Cbl can affect macrophage polarization by regulating M-CSF/M-CSFR/PI3K/AKT signaling pathway.

Materials and methods

Mice

Mice were C57BL/6 background. Cbl-b$^{-/-}$ and c-Cbl$^{flox/flox}$ mice were kindly gifted by Dr. Hua Gu (Montreal Clinic Research Institute, Montreal, Quebec, Canada) [23]. Lyzs-Cre mice were gifted by *Prof.*

Yulong He (Soochow University, China). Lyzs-Cre mice were crossed with c-Cbl$^{flox/flox}$ to generate c-Cbl$^{flox/flox}$ Lyzs-Cre^{+} mice. Subsequently, the progeny was crossed with Cbl-b$^{-/-}$ mice to generate Cbl-b$^{-/-}$ c-Cbl$^{flox/flox}$ Lyzs-Cre^{+} (dKO) mice. All mice were housed under specific pathogen-free conditions at the Soochow University animal facility. 6–8 weeks old mice were used unless indicated with no sex-selective preference. Our study examined male and female animals, and similar findings are reported for both sexes. All animal experiments were performed following the institutional guidelines and approved by the Institutional Animal Use and Care Committee of Soochow University.

Cell culture, maintenance and transfection

Human embryonic kidney (HEK) 293T and MH-S (Mouse alveolar macrophage cell line) cells were purchased from the American Type Culture Collection (ATCC). HEK293T cells cultured in DMEM medium (HyClone, Logan, Utah) containing 10% fetal bovine serum (Gibco, Hong Kong), 100 U/mL penicillin and 100 μg/mL streptomycin (Gibco, Hong Kong). MH-S cells cultured in RPMI 1640 medium (HyClone, Logan, Utah) containing 10% (vol/vol) fetal bovine serum (Gibco, Hong Kong), 100 U/mL penicillin and 100 μg/mL streptomycin (Gibco, Hong Kong). All cells were cultured at 37℃ under 5% CO_2. All transient transfections were carried out using D-porzai (Merit, Tianjin, China) according to manufacturer's instruction.

Histopathology

For histopathology analysis, tissues were fixed more than 24 h in a 4% paraformaldehyde solution (Solarbio, Beijing, China), processed, and then embedded in paraffin (Leica, Germany) according to standard procedures. Next, 5 μm sections were stained with hematoxylin solution (Sigma-Aldrich, USA) for 5–10 min and 0.5% eosin solution (Solarbio, Beijing, China) for 30–90 sec. The Stained sections were scanned using a microscope (ECLIPSE 90i, Nikon, Japan).

Preparation of mouse lung tissue single-cell suspension

Mouse lungs were cut into fine pieces and digested with 0.5 mg/mL collagenase IV (Sigma-Aldrich, USA) and 20 ng/mL DNase I (Solarbio, Beijing, China) in RPMI-1640 medium (HyClone, Logan, Utah) for 1 h at 37°C. The cells were then washed twice with ice-cold 1 × PBS (PROLEADER, Shanghai, China) and erythrocytes were removed using ACK lysis buffer (150 mM NH4Cl, 10 mM KHCO3, 0.1 mM Na2EDTA, pH 7.2–7.4).

Isolation of mouse liver lymphocytes

Mouse livers were cut into fine pieces and digested with 0.5 mg/mL collagenase IV (Sigma-Aldrich, USA) and 20 ng/mL DNase I (Solarbio, Beijing, China) in RPMI-1640 medium (HyClone, Logan, Utah) for 30 min at 37°C. The cells were then washed twice with ice-cold 1 × PBS and resuspended in 10 mL Mouse 1 × Lymphocyte Separation Medium (DAKEWE, Shenzhen, China). Lymphocytes were separated according to the manufacturer's protocol.

Cell staining and flow cytometry

Cells were stained with fluorescence-coupled anti-mouse antibodies listed below diluted in 1 × PBS for 30 min at 4℃ and subsequently washed with 1 × PBS. Analysis was carried out on a BD FACSCanto™ Ⅱ (BD Pharmingen™, USA) while cell sorting was conducted on a BD FACSAria™ Ⅱ (BD Pharmingen™, USA). APC/Cy7-anti-CD11c (N418) (#117324), APC-anti-CD11c (N418) (#117310), PE/Cy7-anti-CD11c (N418) (#117318), PE-anti-CD11b (M1/70) (#101208), FITC-anti-CD11b (M1/70) (#101206), APC-anti-CD45 (30-F11) (#103112), PE-anti-CD64 (X54-5/7.1) (#139304), PerCP/Cy5.5-anti-Siglec-F (S17007L) (#155526), APC-anti-CD24 (clone M1/69) (#101814), FITC-anti-IA/IE (M5/114.15.2) (#107606), PE/Cy7-anti-IA/IE (M5/114.15.2) (#107630), PE-anti-F4/80 (BM8) (#123110), PE/Cy7-anti-Ly-6G (1A8) (#127618), PerCP/Cy5.5-anti-Ly-6G (1A8) (#127616), APC-anti-LY-6C (HK1.4) (#128016), PE-anti-CD115 (AFS98) (#135506), FITC-anti-CD326 (G8.8), PE/Cy7-anti-CD45R/B220 (RA3-6B2) (#103222), APC-anti-CD206 (C068C2) (#141708), FITC-anti-CD86 (GL-1) (#105006), PE/Cy7-anti-CD4 (GK1.5) (#100422), PE/Cy7-anti-CD8a (53 – 6.7) (#100722), PE/Cy7-anti-NK1.1 (PK136) (#108714), APC-anti-Sca-1 (D7) (#108112), PE/Cy7-anti-TER-119/Erythroid Cells (TER-119) (#116222), PE/Cy7-anti-Ly-6G/Ly-6C (Gr-1) (R86-8C5) (#108416), APC/Cy7-anti-c-Kit (2B8) (#105826), PE-anti-CD34 (MEC147) (#119308), APC/Cy7-anti-CD16/32 (93) (#101328) and APC-anti-Flt3/CD135 (A2F10) (#135310) were purchased from BioLegend (San Diego, USA). PE/Cy7-anti-CD11b (M1/70) (#552850), APC-anti-F4/80 (BM8) (#123116) and PE/Cy7-anti-CD3e (145-2C11) (#100220) were purchased from BD Pharmingen™ (USA). Alexa Flour 488®-anti-CX3CR1 (#FAB5825G) were purchased from R&D Systems (USA).

Bronchoalveolar lavage of mice

After euthanized, the bronchoalveolar lavage (BAL) was performed on the whole lungs of mice by 2 ml 1 × PBS (PROLEADER, Shanghai, China) for 6 times with gentle massage. Almost 90% of fluid were recovered. The bronchoalveolar lavage fluid (BALF) was centrifuged at 1000 g for 5 min at 4℃. The supernatant of the BALF stored at -80℃ for enzyme-linked immunosorbent assay (ELISA), and sediments were collected for cell counts and flow cytometry assay.

Isolation of alveolar macrophages (AMs)

AMs were isolated by BALF. BALF was collected and then centrifuged at 1000 g for 5 min at 4°C. The cells were re-suspended with DMEM medium (HyClone, Logan, Utah) containing 10% (vol/vol) fetal bovine serum (Gibco, Hong Kong), 100 U/mL penicillin and 100 μg/mL streptomycin (Gibco, Hong Kong) and inocubated in 10 cm cell culture dishes (NEST, Wuxi, China) for 2–4 h at 37℃. The cells adhering to the bottom of dish were collected for further experimental use.

ELISA

The level of IL-1β, IL-6 and TGF-β in BALF of WT and dKO mice was determined by ELISA (Invitrogen, USA; Biolegend, USA; MEIMIAN, China). 100 μl supernatant of BALF was added per well and the assay was performed according to the protocol of manufacturer. The OD values at 450 nm were detected using Synergy™ H4 (BIO-TEK, USA).

Cell proliferation assay

For BrdU incorporation analysis in vivo, mice aged 6–8 weeks were labeled by two intraperitoneal injections of BrdU. According to the standard of 200 mg/kg, mice were intraperitoneally injected with 200 μL of 10 mg/mL BrdU solution (Sigma-Aldrich, Germany) at 12 h and 4 h before sacrifice. AMs were isolated by BAL as“Isolation of alveolar macrophages”described. The AMs were seeded at a density of 1 × 10^4 cells/well in a 96-well plate (NEST, Wuxi, China) and incubated for 2 h at 37℃. The BrdU Cell Proliferation Assay Kit (CST, Danvers, MA, USA) used an anti-BrdU antibody to detect BrdU incorporated into cellular DNA during cell proliferation and the assay was performed according to the manufacturer's instructions. The OD values at 450 nm were detected using Synergy™ H4 (BIO-TEK, USA).

For BrdU incorporation analysis in vitro, M-CSF-stimulated cells were incubated in RPMI-1640 medium containing 10 μM BrdU (Sigma-Aldrich, Germany) for 4–6 h. The Cells were stained with corresponding antibodies against surface markers and subsequently washed with 1 × PBS. Next, the cells were treated with Cytofix/Cytoperm Fixation and Permeabilization Solution (BD Pharmingen™, USA) overnight at 4℃, digested by DNase I (Solarbio, Beijing, China) for 1 h, intracellular stained with FITC-anti-BRDU (#51-33284X) (BD Pharmingen™, USA) or APC-anti-BrdU (Bu20a) (#339808) (BioLegend, USA) for 30 min at 4℃. After washing with 1 × BD Perm/Wash Buffer (BD Pharmingen™, USA), the cells were run on a BD FACSCanto™ Ⅱ (BD Pharmingen™, USA) and data were analyzed with FlowJo software (Treestar, USA).

Cell apoptosis assay

For the apoptosis analysis, Alveolar macrophages and M-CSF-stimulated cells were first stained with corresponding antibodies against surface markers and subsequently washed with 1 × Annexin V binding buffer (BD Pharmingen™, USA). Next, single cell suspensions were stained with APC-anti-Annexin V (#640941) (Biolegend, USA) or FITC-anti-Annexin V (#51-65874X) (BD Pharmingen™, USA) and PerCP/Cy5.5-anti-7-AAD (#51-68981E) (BD Pharmingen™, USA) in a 1 × Annexin V binding buffer according to the manufacturer’s instruction. Cells were analyzed using a BD FACSCantoTM Ⅱ (BD Pharmingen™, USA). FACS data was quantified using the FlowJo software (Tree Star, USA).

Preparation of BMDMs and cell culture

Femur and tibia were harvested from mice, washed with 1 × PBS and bone marrow cells were flushed out with 1 × PBS. Erythrocytes were removed using ACK lysis buffer (150 mM NH4Cl, 10 mM KHCO3, 0.1 mM Na2EDTA, pH 7.2–7.4). The cell suspension was filtered through 70 μm cell strainer to remove any cell clumps and impurities. The single cell suspension was then cultured at a density of 2 × 10^6 cells/mL in RPMI-1640 medium (HyClone, Logan, Utah) containing 10% (vol/vol) fetal bovine serum (Gibco, Hong Kong), 100 U/mL penicillin, 100 μg/mL streptomycin (Gibco, Hong Kong) and 20 ng/ml recombinant murine M-CSF (Peprotech, USA). Fresh medium containing M-CSF was added on day 3, half of the medium containing M-CSF was exchanged on day 5, and the fully differentiated BMDMs were harvested on day 7 for function assay. For M-CSFR inhibitor treatment, different concentrations of the M-CSFR inhibitor BLZ945 (Sotuletinib, MedChemExpress, USA) were added to the culture system for 7 d. The inhibitor was replenished with media exchanges.

Adoptive transfer mouse model

In the AMs adoptive transfer experiment, 6–8 weeks old WT mice in a C57BL/6 background were irradiated and injected intravenously with BALF AMs purified from WT or dKO mice (2×10^6 cells). Injections were carried out 3 times, once every 5 days. After two weeks, mice were sacrificed to assess pathologic lung changes via Hematoxylin and eosin (H&E) staining.

In the BMDMs adoptive transfer experiment, 6–8 weeks old WT mice in a C57BL/6 background were irradiated and injected intravenously with BMDMs induced from the bone marrow of WT or dKO mice (2×10^6 cells). Injections were carried out 4 times, once every 5 days. After three weeks, mice were sacrificed to assess pathologic lung changes via Hematoxylin and eosin (H&E) staining.

Western blotting

Cell lysates were obtained from cultured cells using NP-40 lysis buffer (Beyotime, Shanghai, China) containing 1 mM protease inhibitors PMSF (Beyotime, Shanghai, China) for 20–30 min on ice. The BCA Protein Assay Kit (Thermo Fisher Scientific, USA) was used to quantify protein concentration in the samples. Prior to loading, 5 × SDS loading buffer (NCM Biotech, Suzhou, China) was added to protein lysates and the samples were boiled for 10 min. Equivalent amount of proteins were subjected to SDS-PAGE gel and then were transferred to PVDF membranes (Millipore, Germany). Membranes were blocked with 5% nonfat milk (Bio Basic, Shanghai, China) or 2% BSA for 1 h at room temperature, and then incubated with the primary antibodies overnight at 4°C. After washing three times with 0.1% PBST (1 × PBS and 0.1% Tween 20), the membranes were subjected to secondary antibodies (HRP-conjugated Affinipure Goat Anti-Mouse IgG [Proteintech, USA] or Goat Anti-Rabbit IgG-HRP [Sourthern Biotech, USA]) in 5% nonfat milk (Bio Basic, Shanghai, China) for 1 h at room temperature. After washing three times with 0.1% PBST, the membranes were treated with enhanced chemiluminescence (ECL) reagents (Bio-Rad, USA), and protein bands were observed by exposure to X-ray films (FUJIFILM, Japan). The following antibodies (Clone) with dilutions were used in our study: anti-Cbl-b (D3C12) (#9498, 1:1000), anti-c-Cbl (D4E10) (#8447, 1:1000), anti-M-CSFR (E6W9F) (#43390, 1:1000), anti-Myc (9B11) (#2276, 1:1000), anti-His (D3I1O) (#12698, 1;1000), anti-AKT (C67E7) (#4691, 1:1000), anti-p-AKT (D7F10) (#9018, 1:1000), anti-Erk1/2 (137F5) (#4695, 1:1000), anti-p-Erk (D13.14.4E) (#4370, 1:1000), anti-Phospho-Tyrosine (4G10) (#96215, 1:1000), anti-Caspase-9 (#9504, 1:1000), anti-Caspase-8 (#4927, 1:1000), anti-Caspase-7 (#9492, 1:1000), anti-Cleaved Caspase-7 (Asp198) (#9491, 1:1000), anti-Caspase-3 (D3R6Y) (#14220, 1:1000), anti-Cleaved Caspase-3 (5A1E) (#9664, 1:1000), anti-Bim (C34C5) (#2933, 1:1000), anti-Bcl-xL (54H6) (#2764, 1:1000) and anti-K63-linkage Specific Polyubiquitin (D7A11) (#5261, 1:1000), all antibodies purchased from Cell Signaling Technology (Danvers, MA, USA). Anti-Ubiquitin (P4D1) (#G2618, 1:1000) antibody was purchased from Santa Cruz (USA). Anti-HA (#T0050, 1:1000) and anti-β-Actin (#T0022, 1:5000) antibodies were purchased from Affinity Biosciences (USA).

Immunoprecipitation

Cells were harvested in NP-40 lysis buffer (Beyotime, Shanghai, China) containing containing 1 mM protease inhibitors PMSF (Beyotime, Shanghai, China). When protein ubiquitination was examined, 10 mM N-ethylmaleimide (MedChemExpress, USA) was added into the NP-40 lysis buffer. When protein phosphorylation was examined, 1 × phosphatase inhibitor (Beyotime, Shanghai, China) was added into the NP-40 lysis buffer. The cell lysates were incubated with corresponding specific antibodies overnight on a rotor at 4℃. Protein G-Agarose beads (Roche Diagnostics GmbH, Mannheim, Germany) were washed thrice with NP-40 wash buffer (5 M NaCl, 1 M Tris-HCl, pH 7.4, 1% Noidet P-40) and then were added into the supernatant. The mixture was incubated for 4–6 h on a rotor at 4℃. Immunoprecipitates were washed once with NP-40 wash buffer, once with High Salt buffer (5 M NaCl, 0.05% Triton X-100, 1 × PBS), and finally once with NP-40 washing buffer. After boiling with 60 μL loading buffer (NP-40 wash buffer, 5× SDS loading buffe) for 10 min, the immunoprecipitates were analyzed by western blot.

M-CSFR ubiquitination and degradation assays

For in vitro M-CSFR ubiquitination and degradation assays, HEK293T cells transfected with indicated overexpressed plasmids. 24 h later, transfected cells were treated with or without 50 ng/ml M-CSF at 37°C for 2 h. For protein degradation assay, new protein synthesis was blocked by 50 μM CHX (SelleckChem, USA). For protein degradation pathway assay, 10 μM MG132 (Sigma-Aldrich, USA) and 20 μM CQ (MedChemExpress, USA) were used to block protein degradation, respectively. For protein ubiquitination assay, protein degradation was blocked with 20 μM CQ (MedChemExpress, USA) for 15 min before stimulation with M-CSF. Exogenous M-CSFR ubiquitination and expression were then analyzed by Imunoprecipitation and Western blot analysis using indicated antibodies.

For in vivo M-CSFR degradation assays, the fully differentiated BMDMs were incubated at 37°C without M-CSF for 16–24 h. Cells were then stimulated with or without 50 ng/ml M-CSF at 37°C for indicated time. For in vivo M-CSFR ubiquitination assays, the fully differentiated BMDMs were incubated at 37°C without M-CSF for 16–24 h. Next, BMDMs stimulated with or without 50 ng/ml M-CSF at 37°C for 1–3 min and M-CSFR degradation was blocked with 20 μM CQ for 15 min before stimulation with M-CSF. Endogenous M-CSFR ubiquitination and expression were then analyzed by Imunoprecipitation and Western blot analysis using indicated antibodies.

Real-time PCR

Total RNA was extracted from purified BALF AMs or mouse lung tissue using the RNA isolater Total RNA Extraction Reagent (Vazyme, Nanjing, China). First-strand complementary DNAs (cDNAs) were synthesized using the HiScript III RT SuperMix for qPCR (+ gDNA wiper) (YEASEN, Shanghai, China). QPCR was performed on a QuantStudio 1 real-time fluorescence quantitative PCR system (Thermo Fisher Scientific, USA). Quantification of all target genes was carried out by normalizing to the control gene β-actin or 18S. The sequences of primers used in Real-time PCR are listed in Table S1. All primers were synthesized by Azenta (GENEWIZ, Suzhou, China).

Plasmids and reagents

HA ubiquitin (HA-Ub), HA-K6 (all lysines on the ubiquitin gene are mutated to arginines except 6), HA-K11 (all lysines on the ubiquitin gene are mutated to arginines except 11), HA-K27 (all lysines on the ubiquitin gene are mutated to arginines except 27), HA-K29 (all lysines on the ubiquitin gene are mutated to arginines except 29), HA-K33 (all lysines on the ubiquitin gene are mutated to arginines except 33), HA-K48 (all lysines on the ubiquitin gene are mutated to arginines except 48) and HA-K63(all lysines on the ubiquitin gene are mutated to arginines except 63) plasmids were gifts from Dr. Hui Zheng of Institutes of Biology and Medical Sciences (Soochow University, Suzhou, China). Sequences coding for Cbl-b and c-Cbl were amplified from C57BL/6J mouse thymus cDNA and cloned into pcDNA3.1 + basic vector between the KpnI and XhoI sites. Sequences coding for M-CSFR was amplified from C57BL/6J mouse splenic cDNA and cloned into pcDNA3.1- basic vector between the EcoRI and XhoI sites. The sequences of primers used for cloning are shown in Table S2. Five Cbl-b (C373A, Y363F, Y664F, Y708F and Y889F), six c-Cbl (C379A, Y369F, Y672F, Y698F, Y737F and Y780F) and fifteen M-CSFR (K614M, Y544F, Y559F, Y697F, Y706F, Y721F, Y807F, Y921F, Y974F, K572R, K584R, K604R, K698R, K791R and K868R) mutations were generated using the 2 × Phanta Max Master Mix (Vazyme, Nanjing, China) and FastDigest DpnI (Thermo Fisher Scientific, Lithuania) according to the manufacturer's instructions. Primers used for Cbl-b and c-Cbl mutations are shown in Table S3 and primers used for M-CSFR mutations are shown in Table S4.

Statistical analysis

Biological replicates were performed for all experiments as indicated. Prism 8 (GraphPad) was used for statistical analysis. To assess the statistical significance of different treatment groups, we used One-Way ANOVA comparisons or unpaired two-tailed Student's *t* tests in two different treatments. For survival curve analysis, log-rank tests were performed. *indicated $p < 0.05$; **$p < 0.01$; ***$p < 0.001$, ****$p < 0.0001$, ns indicates not significant. *p* values less than 0.05 were considered statistically significant. Data represent three independent experiments unless indicated. Values for all data points in graphs are reported in the Supporting Data Values file.

Declarations

Acknowledgments

This work was supported by grants from the National Natural Science Foundation of China (grant numbers: 81771667, 81970027, 82170012, 82070009, 82071765, 82370020, 82270018), Social Development Project of Jiangsu Province (grant number: BE2019671, BE2016676), Jiangsu Key Laboratory of Infection and Immunity, Institutes of Biology and Medical Sciences of Soochow University, Key Lab of Respiratory Disease of Suzhou (grant number: SZS201714), Key Laboratory for Diagnosis and Treatment of Immune Diseases in Children (grant number: SZS201808), Clinician scientist Project of Suzhou Medical College (ML13100323), the Priority Academic Program Development of Jiangsu Higher Education Institutions and Suzhou International Joint Laboratory for Diagnosis and Treatment of Brain Diseases.

Author Contributions

JZ, YY, and CLH conceived and supervised the study and provided funding and critical reagents. FX and CST designed and performed most of the experiments and wrote the manuscript. KT, GDQ, YS, XPL, PJZ and JMC prepared the figures and performed part of the mice experiments. MYW, XG, JZ and ZRC assisted with the reagents preparation, transfections and co-immunoprecipitation experiments. YFW and BBH performed part of the molecular mechanisms experiments. JPZ initiated this project. All authors approved the final version of the paper.

Competing Financial Interests

The authors declare no competing financial interests.

References

1. Martinez, F.O., L. Helming, and S. Gordon, *Alternative activation of macrophages: an immunologic functional perspective.* Annu Rev Immunol, 2009. **27**: p. 451-83.
2. Epelman, S., K.J. Lavine, and G.J. Randolph, *Origin and functions of tissue macrophages.* Immunity, 2014. **41**(1): p. 21-35.
3. Peiró, T., et al., *Neutrophils drive alveolar macrophage IL-1β release during respiratory viral infection.* Thorax, 2018. **73**(6): p. 546-556.
4. Li, F., et al., *Gene therapy of Csf2ra deficiency in mouse fetal monocyte precursors restores alveolar macrophage development and function.* JCI Insight, 2022. **7**(7).
5. Kopf, M., C. Schneider, and S.P. Nobs, *The development and function of lung-resident macrophages and dendritic cells.* Nat Immunol, 2015. **16**(1): p. 36-44.
6. Bhargava, A., M. Vagela, and C.M. Lennox, *"Challenges in the management of fractures in osteopetrosis"! Review of literature and technical tips learned from long-term management of seven patients.* Injury, 2009. **40**(11): p. 1167-71.
7. Strickland, J.P. and D.J. Berry, *Total joint arthroplasty in patients with osteopetrosis: a report of 5 cases and review of the literature.* J Arthroplasty, 2005. **20**(6): p. 815-20.
8. Hamilton, J.A., *Colony-stimulating factors in inflammation and autoimmunity.* Nat Rev Immunol, 2008. **8**(7): p. 533-44.
9. Chitu, V. and E.R. Stanley, *Colony-stimulating factor-1 in immunity and inflammation.* Curr Opin Immunol, 2006. **18**(1): p. 39-48.
10. Stanley, E.R., et al., *Biology and action of colony--stimulating factor-1.* Mol Reprod Dev, 1997. **46**(1): p. 4-10.
11. Wiktor-Jedrzejczak, W., et al., *CSF-1 deficiency in the op/op mouse has differential effects on macrophage populations and differentiation stages.* Exp Hematol, 1992. **20**(8): p. 1004-10.
12. Hamilton, J.A., *CSF-1 signal transduction.* J Leukoc Biol, 1997. **62**(2): p. 145-55.

13. Pixley, F.J. and E.R. Stanley, *CSF-1 regulation of the wandering macrophage: complexity in action.* Trends Cell Biol, 2004. **14**(11): p. 628-38.
14. Lee, A.W. and D.J. States, *Colony-stimulating factor-1 requires PI3-kinase-mediated metabolism for proliferation and survival in myeloid cells.* Cell Death Differ, 2006. **13**(11): p. 1900-14.
15. Smith, J.L., et al., *ets-2 is a target for an akt (Protein kinase B)/jun N-terminal kinase signaling pathway in macrophages of motheaten-viable mutant mice.* Mol Cell Biol, 2000. **20**(21): p. 8026-34.
16. Lee, A.W., *Synergistic activation of mitogen-activated protein kinase by cyclic AMP and myeloid growth factors opposes cyclic AMP's growth-inhibitory effects.* Blood, 1999. **93**(2): p. 537-53.
17. Rao, N., I. Dodge, and H. Band, *The Cbl family of ubiquitin ligases: critical negative regulators of tyrosine kinase signaling in the immune system.* J Leukoc Biol, 2002. **71**(5): p. 753-63.
18. Thien, C.B. and W.Y. Langdon, *Cbl: many adaptations to regulate protein tyrosine kinases.* Nat Rev Mol Cell Biol, 2001. **2**(4): p. 294-307.
19. Keane, M.M., et al., *Cloning and characterization of cbl-b: a SH3 binding protein with homology to the c-cbl proto-oncogene.* Oncogene, 1995. **10**(12): p. 2367-77.
20. Keane, M.M., et al., *cbl-3: a new mammalian cbl family protein.* Oncogene, 1999. **18**(22): p. 3365-75.
21. Jeon, M.S., et al., *Essential role of the E3 ubiquitin ligase Cbl-b in T cell anergy induction.* Immunity, 2004. **21**(2): p. 167-77.
22. Naramura, M., et al., *c-Cbl and Cbl-b regulate T cell responsiveness by promoting ligand-induced TCR down-modulation.* Nat Immunol, 2002. **3**(12): p. 1192-9.
23. Li, X., et al., *Cbl Ubiquitin Ligases Control B Cell Exit from the Germinal-Center Reaction.* Immunity, 2018. **48**(3): p. 530-541.e6.
24. Kitaura, Y., et al., *Control of the B cell-intrinsic tolerance programs by ubiquitin ligases Cbl and Cbl-b.* Immunity, 2007. **26**(5): p. 567-78.
25. Chiou, S.H., et al., *The E3 ligase c-Cbl regulates dendritic cell activation.* EMBO Rep, 2011. **12**(9): p. 971-9.
26. Huang, F. and H. Gu, *Negative regulation of lymphocyte development and function by the Cbl family of proteins.* Immunol Rev, 2008. **224**: p. 229-38.
27. Liu, Y.C. and H. Gu, *Cbl and Cbl-b in T-cell regulation.* Trends Immunol, 2002. **23**(3): p. 140-3.
28. Tong, H., et al., *Ubiquitin Ligases CBL and CBL-B Maintain the Homeostasis and Immune Quiescence of Dendritic Cells.* Front Immunol, 2021. **12**: p. 757231.
29. Xu, F., et al., *Ablation of Cbl-b and c-Cbl in dendritic cells causes spontaneous liver cirrhosis via altering multiple properties of CD103(+) cDC1s.* Cell Death Discov, 2022. **8**(1): p. 142.
30. Yu, W., et al., *CSF-1 receptor structure/function in MacCsf1r-/- macrophages: regulation of proliferation, differentiation, and morphology.* J Leukoc Biol, 2008. **84**(3): p. 852-63.
31. Suzu, S., et al., *M-CSF-mediated macrophage differentiation but not proliferation is correlated with increased and prolonged ERK activation.* J Cell Physiol, 2007. **212**(2): p. 519-25.

32. Audu, C.O., et al., *Macrophage-specific inhibition of the histone demethylase JMJD3 decreases STING and pathologic inflammation in diabetic wound repair.* Cell Mol Immunol, 2022. **19**(11): p. 1251-1262.
33. Davis, F.M., et al., *Histone Methylation Directs Myeloid TLR4 Expression and Regulates Wound Healing following Cutaneous Tissue Injury.* J Immunol, 2019. **202**(6): p. 1777-1785.
34. Menon, M.B., et al., *Lyz2-Cre-Mediated Genetic Deletion of Septin7 Reveals a Role of Septins in Macrophage Cytokinesis and Kras-Driven Tumorigenesis.* Front Cell Dev Biol, 2021. **9**: p. 795798.
35. Negretti, N.M., et al., *A single-cell atlas of mouse lung development.* Development, 2021. **148**(24).
36. Stanley, E.R. and V. Chitu, *CSF-1 receptor signaling in myeloid cells.* Cold Spring Harb Perspect Biol, 2014. **6**(6).
37. Guilbert, L.J. and E.R. Stanley, *Specific interaction of murine colony-stimulating factor with mononuclear phagocytic cells.* J Cell Biol, 1980. **85**(1): p. 153-9.
38. Yeung, Y.G., et al., *Purification of the colony-stimulating factor 1 receptor and demonstration of its tyrosine kinase activity.* Proc Natl Acad Sci U S A, 1987. **84**(5): p. 1268-71.
39. Dai, X.M., et al., *Targeted disruption of the mouse colony-stimulating factor 1 receptor gene results in osteopetrosis, mononuclear phagocyte deficiency, increased primitive progenitor cell frequencies, and reproductive defects.* Blood, 2002. **99**(1): p. 111-20.
40. Sakagami, T., et al., *Human GM-CSF autoantibodies and reproduction of pulmonary alveolar proteinosis.* N Engl J Med, 2009. **361**(27): p. 2679-81.
41. Wang, Y., et al., *IL-34 is a tissue-restricted ligand of CSF1R required for the development of Langerhans cells and microglia.* Nat Immunol, 2012. **13**(8): p. 753-60.
42. Meshkibaf, S., et al., *G-CSF preferentially supports the generation of gut-homing Gr-1high macrophages in M-CSF-treated bone marrow cells.* J Leukoc Biol, 2014. **96**(4): p. 549-61.
43. Duplomb, L., et al., *Interleukin-6 inhibits receptor activator of nuclear factor kappaB ligand-induced osteoclastogenesis by diverting cells into the macrophage lineage: key role of Serine727 phosphorylation of signal transducer and activator of transcription 3.* Endocrinology, 2008. **149**(7): p. 3688-97.
44. Yin, Z., et al., *IL-6/STAT3 pathway intermediates M1/M2 macrophage polarization during the development of hepatocellular carcinoma.* J Cell Biochem, 2018. **119**(11): p. 9419-9432.
45. Eskandari, E. and C.J. Eaves, *Paradoxical roles of caspase-3 in regulating cell survival, proliferation, and tumorigenesis.* J Cell Biol, 2022. **221**(6).
46. Nozaki, K., et al., *Caspase-7 activates ASM to repair gasdermin and perforin pores.* Nature, 2022. **606**(7916): p. 960-967.
47. Amacher, J.F., et al., *Phosphorylation control of the ubiquitin ligase Cbl is conserved in choanoflagellates.* Protein Sci, 2018. **27**(5): p. 923-932.
48. Dou, H., et al., *Structural basis for autoinhibition and phosphorylation-dependent activation of c-Cbl.* Nat Struct Mol Biol, 2012. **19**(2): p. 184-92.

49. Shibata, Y., et al., *Alveolar macrophage deficiency in osteopetrotic mice deficient in macrophage colony-stimulating factor is spontaneously corrected with age and associated with matrix metalloproteinase expression and emphysema.* Blood, 2001. **98**(9): p. 2845-52.
50. Gschwend, J., et al., *Alveolar macrophages rely on GM-CSF from alveolar epithelial type 2 cells before and after birth.* J Exp Med, 2021. **218**(10).
51. Lee, P.S., et al., *The Cbl protooncoprotein stimulates CSF-1 receptor multiubiquitination and endocytosis, and attenuates macrophage proliferation.* Embo j, 1999. **18**(13): p. 3616-28.
52. Rauh, M.J., et al., *SHIP represses the generation of alternatively activated macrophages.* Immunity, 2005. **23**(4): p. 361-74.
53. Kapeller, R. and L.C. Cantley, *Phosphatidylinositol 3-kinase.* Bioessays, 1994. **16**(8): p. 565-76.
54. Marte, B.M. and J. Downward, *PKB/Akt: connecting phosphoinositide 3-kinase to cell survival and beyond.* Trends Biochem Sci, 1997. **22**(9): p. 355-8.
55. Martinez, F.O., et al., *Transcriptional profiling of the human monocyte-to-macrophage differentiation and polarization: new molecules and patterns of gene expression.* J Immunol, 2006. **177**(10): p. 7303-11.
56. Tarique, A.A., et al., *Phenotypic, functional, and plasticity features of classical and alternatively activated human macrophages.* Am J Respir Cell Mol Biol, 2015. **53**(5): p. 676-88.
57. Lu, C.S., et al., *Oct4 promotes M2 macrophage polarization through upregulation of macrophage colony-stimulating factor in lung cancer.* J Hematol Oncol, 2020. **13**(1): p. 62.
58. Chengling, L., et al., *miR-325-3p, a novel regulator of osteoclastogenesis in osteolysis of colorectal cancer through targeting S100A4.* Mol Med, 2021. **27**(1): p. 23.
59. Jones, C.V. and S.D. Ricardo, *Macrophages and CSF-1: implications for development and beyond.* Organogenesis, 2013. **9**(4): p. 249-60.
60. McMahon, K.A., et al., *Colony-stimulating factor-1 (CSF-1) receptor-mediated macrophage differentiation in myeloid cells: a role for tyrosine 559-dependent protein phosphatase 2A (PP2A) activity.* Biochem J, 2001. **358**(Pt 2): p. 431-6.
61. Zhang, C., et al., *Inhibition of tumor growth and metastasis by photoimmunotherapy targeting tumor-associated macrophage in a sorafenib-resistant tumor model.* Biomaterials, 2016. **84**: p. 1-12.
62. Xie, L., et al., *Cationic polysaccharide spermine-pullulan drives tumor associated macrophage towards M1 phenotype to inhibit tumor progression.* Int J Biol Macromol, 2019. **123**: p. 1012-1019.
63. Sarrazin, S., et al., *MafB restricts M-CSF-dependent myeloid commitment divisions of hematopoietic stem cells.* Cell, 2009. **138**(2): p. 300-13.
64. Hume, D.A. and K.P. MacDonald, *Therapeutic applications of macrophage colony-stimulating factor-1 (CSF-1) and antagonists of CSF-1 receptor (CSF-1R) signaling.* Blood, 2012. **119**(8): p. 1810-20.
65. Bonelli, S., et al., *Beyond the M-CSF receptor - novel therapeutic targets in tumor-associated macrophages.* Febs j, 2018. **285**(4): p. 777-787.

66. El-Gamal, M.I., et al., *Recent Advances of Colony-Stimulating Factor-1 Receptor (CSF-1R) Kinase and Its Inhibitors.* J Med Chem, 2018. **61**(13): p. 5450-5466.
67. Wesolowski, R., et al., *Phase Ib study of the combination of pexidartinib (PLX3397), a CSF-1R inhibitor, and paclitaxel in patients with advanced solid tumors.* Ther Adv Med Oncol, 2019. **11**: p. 1758835919854238.

Figures

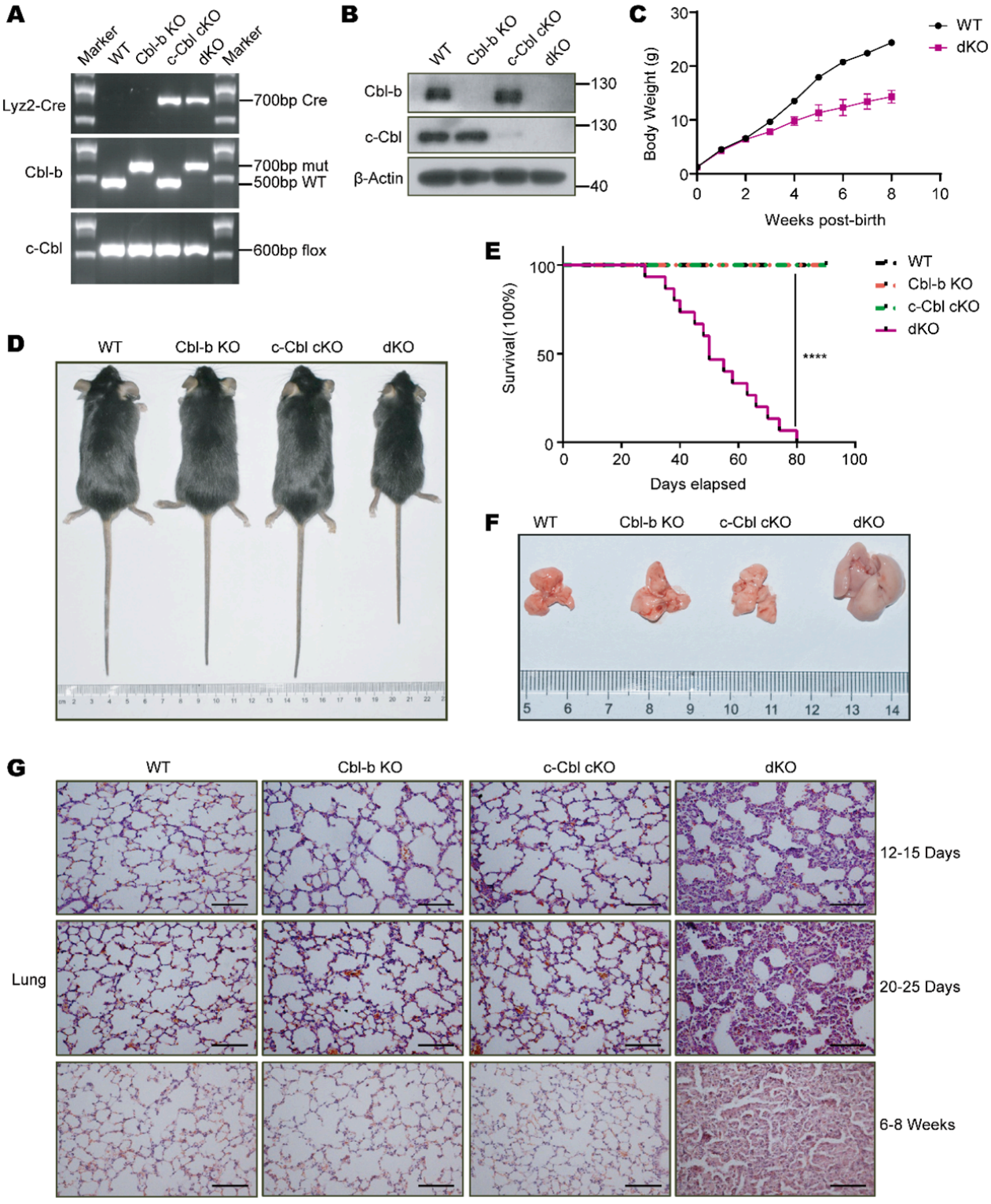

Figure 1

Cbl-b and c-Cbl-deficient mice develop severe lung disease.

(**A**) Genomic DNA was extracted and PCR was performed to detect levels of Lyz2, Cbl-b and c-Cbl in WT,Cbl-b KO, c-Cbl cKO and dKO mice.

(**B**) Western blot analysis of Cbl-b and c-Cbl expression in WT, Cbl-b KO, c-Cbl cKO and dKO BMDMs.

(**C**) The body weight of WT and dKO mice aged 0 to 8 weeks was measured. n=5 per group. The data represent the mean ± SD throughout the figures.

(**D**) The appearance of four groups of mice. The mice shown are 6 weeks in age.

(**E**) Survival curves of four groups of mice. n=15 per group.

(**F**) Lungs of mice of all four genotypes were dissected for morphologic examination. n=3 per group. (**G**) Microscopy of hematoxylin and eosin staining of lung sections from four groups of mice at different ages (n=3 per group); scale bar, 100 μm. *ns*, no significance, *p<0.05, **p<0.01, ***p<0.001, ****p<0.0001. p<0.05 was considered statistically significant.

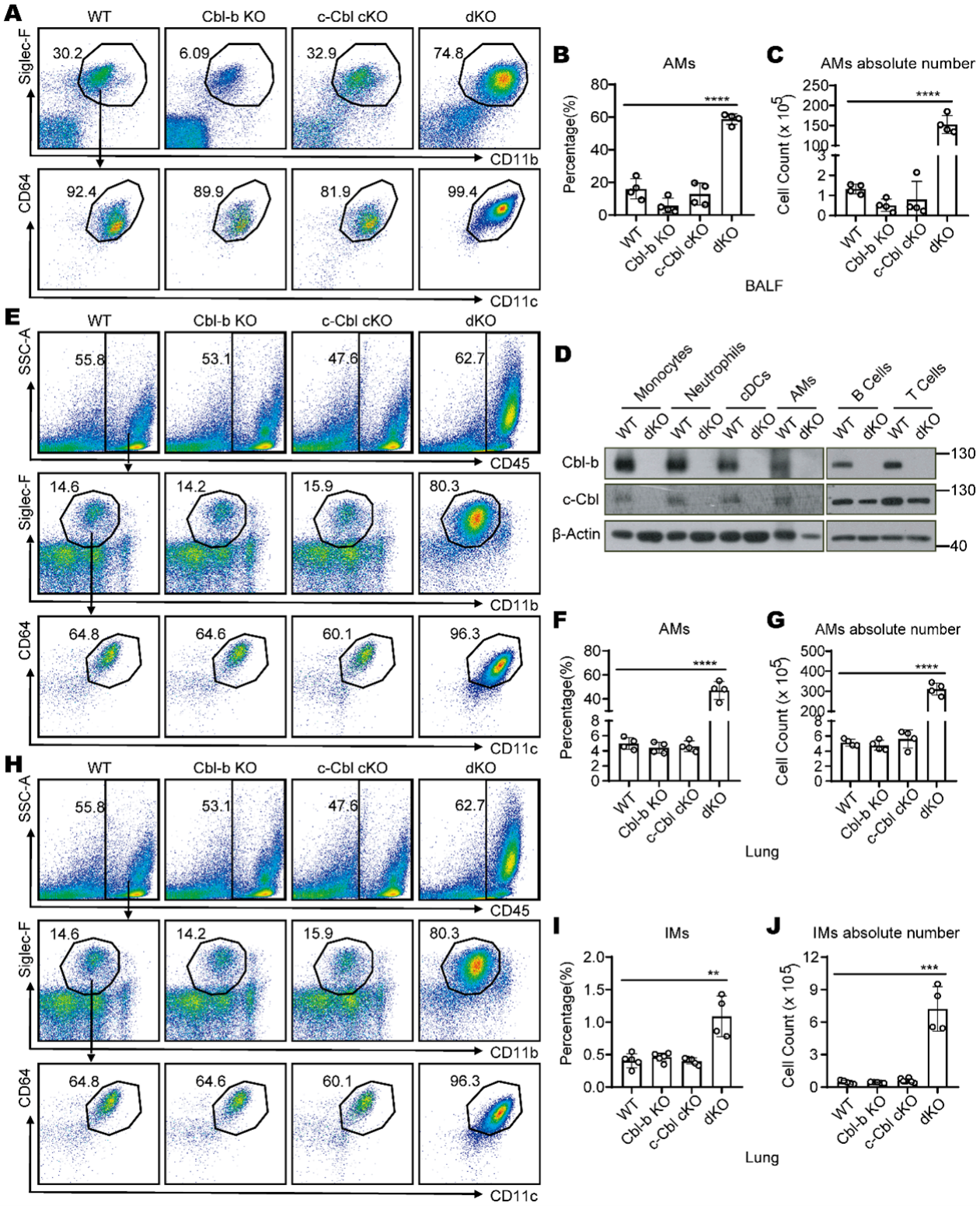

Figure 2

Macrophages were accumulated in dKO lung.

(**A**) Flow cytometry analysis of alveolar macrophages (AMs) (Siglec-F$^+$ CD11b$^+$ CD64$^+$ CD11c$^+$) in BALF (Bronchoalveolar lavage fluid) from four groups of mice. n=4 per group.

(**B and C**) Statistics of percentage (**B**) and absolute number (**C**) of AMs in BALF from four groups of mice, as shown in A.

(**D**) Western blot analysis of Cbl-b and c-Cbl expression in WT and dKO monocytes, neutrophils, cDCs, AMs, B and Tcells.

(**E**) Flow cytometry analysis of AMs ($CD45^+$ $Siglec\text{-}F^+$ $CD11b^{int}$ $CD64^+$ $CD11c^+$) in lungs from four groups of mice. n=4 per group.

(**F and G**) Statistics of percentage (**F**) and absolute number (**G**) of AMs in lungs from four groups of mice, as shown in E.

(**H**) Flow cytometry analysis of interstitial macrophages (IMs) ($CD11c^+$ IA/IE^+ $CD24^-$ $Siglec\text{-}F^-$ $CD11b^{high}$) in lungs from four groups of mice. n=4 per group.

(**I and J**) Statistics of percentage (**I**) and absolute number (**J**) of IMs in lungs from four groups of mice, as shown in H. *ns*, no significance, **p*<0.05, ***p*<0.01, ****p*<0.001, *****p*<0.0001. *p*<0.05 was considered statistically significant.

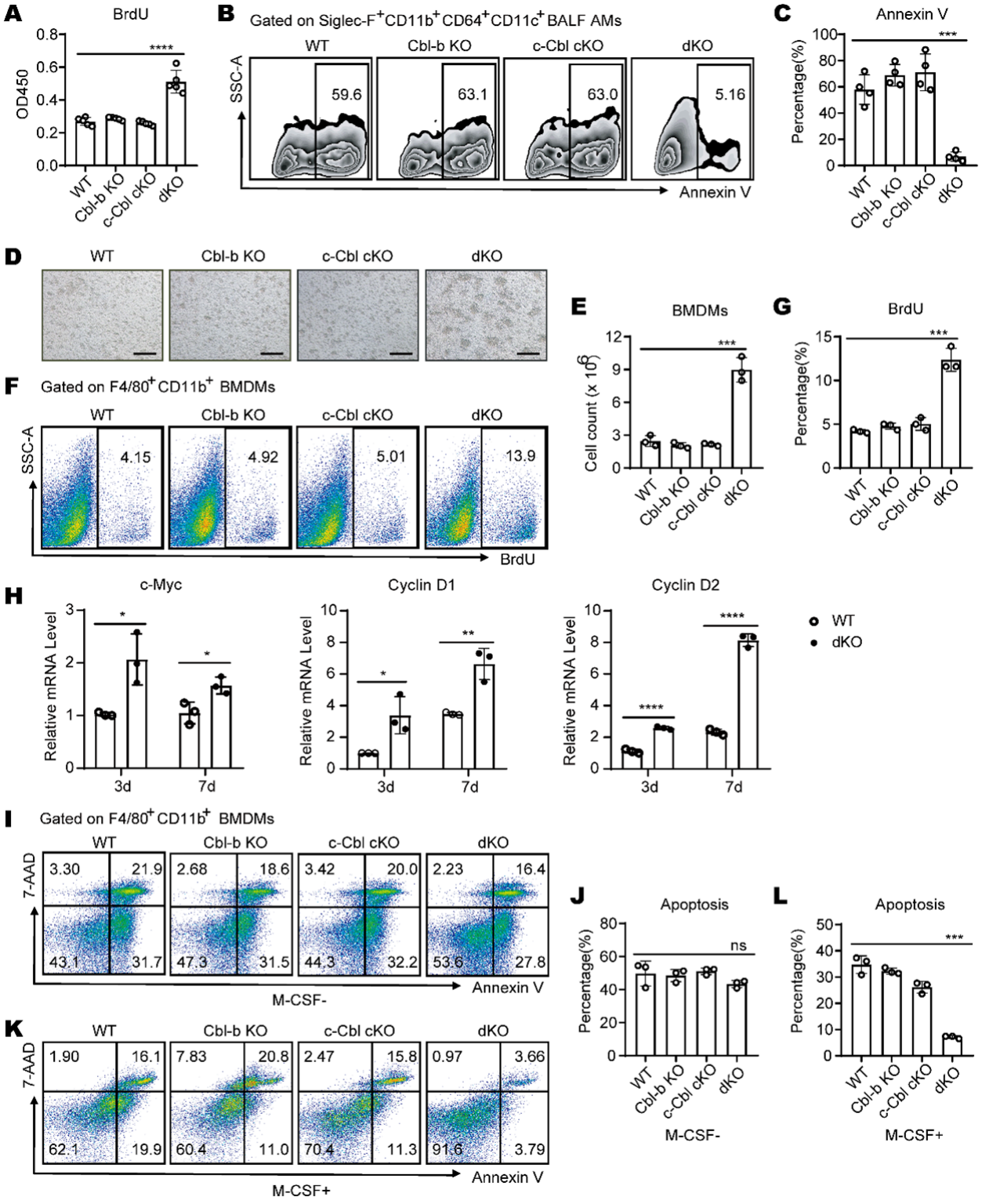

Figure 3

Hyper-proliferation and impaired apoptosis of dKO macrophages contribute to the accumulation of macrophages in mice.

(**A**) Mice were injected with 1 mg BrdU 24 h and 6 h prior to sacrifice, respectively. Proliferation of AMs in BALF from four groups of mice was quantified using BrdU Cell Proliferation Assay Kit. n=5 per group.

(**B**) Flow cytometry analysis of Annexin V^+ AMs in BALF from four groups of mice. n=4 per group.

(**C**) Statistics of percentage of Annexin V^+ AMs in BALF from four groups of mice, as shown in B.

(**D**) Microscopy of clonal morphology of WT, Cbl-b KO, c-Cbl cKO and dKO BMDMs generated in M-CSF dependent BM cell culture; scale bar, 100 μm.

(**E**) Statistics of absolute number of WT, Cbl-b KO, c-Cbl cKO and dKO BMDMs generated in M-CSF dependent BM cell culture. n=3 per group.

(**F and G**) Proliferation of WT, Cbl-b KO, c-Cbl cKO and dKO BMDMs generated in M-CSF dependent BM cell culture. Shown are FACS analyses (**F**) and statistics (**G**) of $BrdU^+$ $F4/80^+$ $CD11b^+$ cells. n = 3 per group.

(**H**) Quantitative PCR analysis of the expression levels of cell cycle-related genes *c-Myc*, *cyclin D1* and *cyclin D2* in WT and dKO BMDMs cultured in the presence of M-CSF (20 ng/mL) for the indicated times.

(**I and J**) WT, Cbl-b KO, c-Cbl cKO and dKO BMDMs were cultured in the presence of M-CSF (20ng/mL) for 5 days, followed by culturing in M-CSF-free medium for another 2 days. Then apoptosis rates were analyzed by flow cytometry. FACS analyses (**I**) and statistics (**J**) of Annexin V^+ $7AAD^-$ and Annexin V^+ $7AAD^+$ $F4/80^+$ $CD11b^+$ cells. n = 3 per group.

(**K and L**) WT, Cbl-b KO, c-Cbl cKO and dKO BMDMs were cultured in the presence of M-CSF (20ng/mL) for 7 days. Then apoptosis rates were analyzed by flow cytometry. FACS analyses (**K**) and statistics (**L**) of Annexin V^+ $7AAD^-$ and Annexin V^+ $7AAD^+$ $F4/80^+$ $CD11b^+$ cells. n = 3 per group. *ns*, no significance, **p*<0.05, ***p*<0.01, ****p*<0.001, *****p*<0.0001. *p*<0.05 was considered statistically significant.

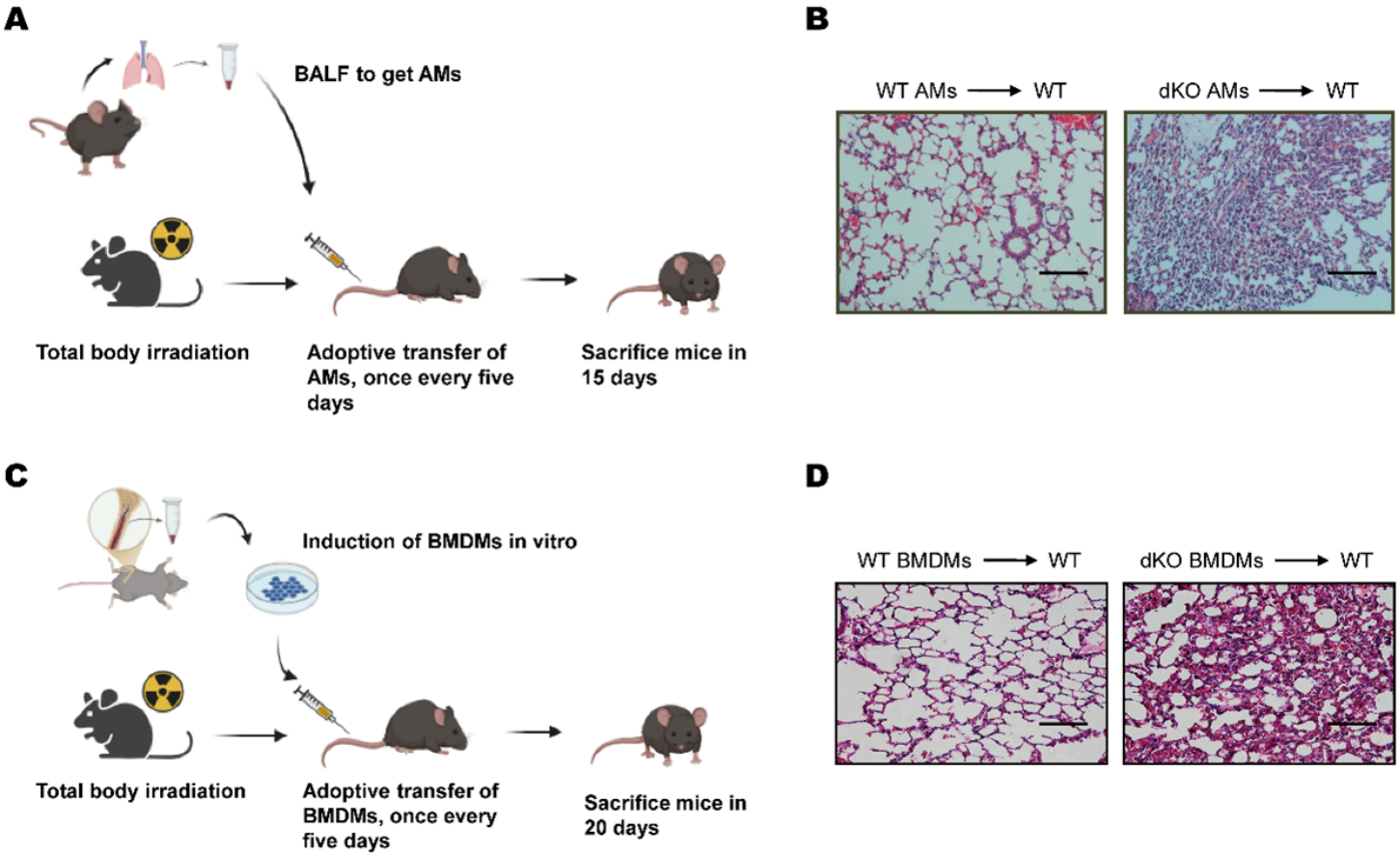

Figure 4

DKO AMs contribute to lung disease and injury.

(**A and B**) BALF AMs purified from WT or dKO mice were adoptively transferred into WT recipient mice respectively, and lung sections were stained with hematoxylin and eosin (n=3 per group); scale bar, 100 μm. (**C and D**) BMDMs induced from WT or dKO mice bone marrow were adoptively transferred into WT recipient mice respectively, and lung sections were stained with hematoxylin and eosin (n=3 per group); scale bar, 100 μm.

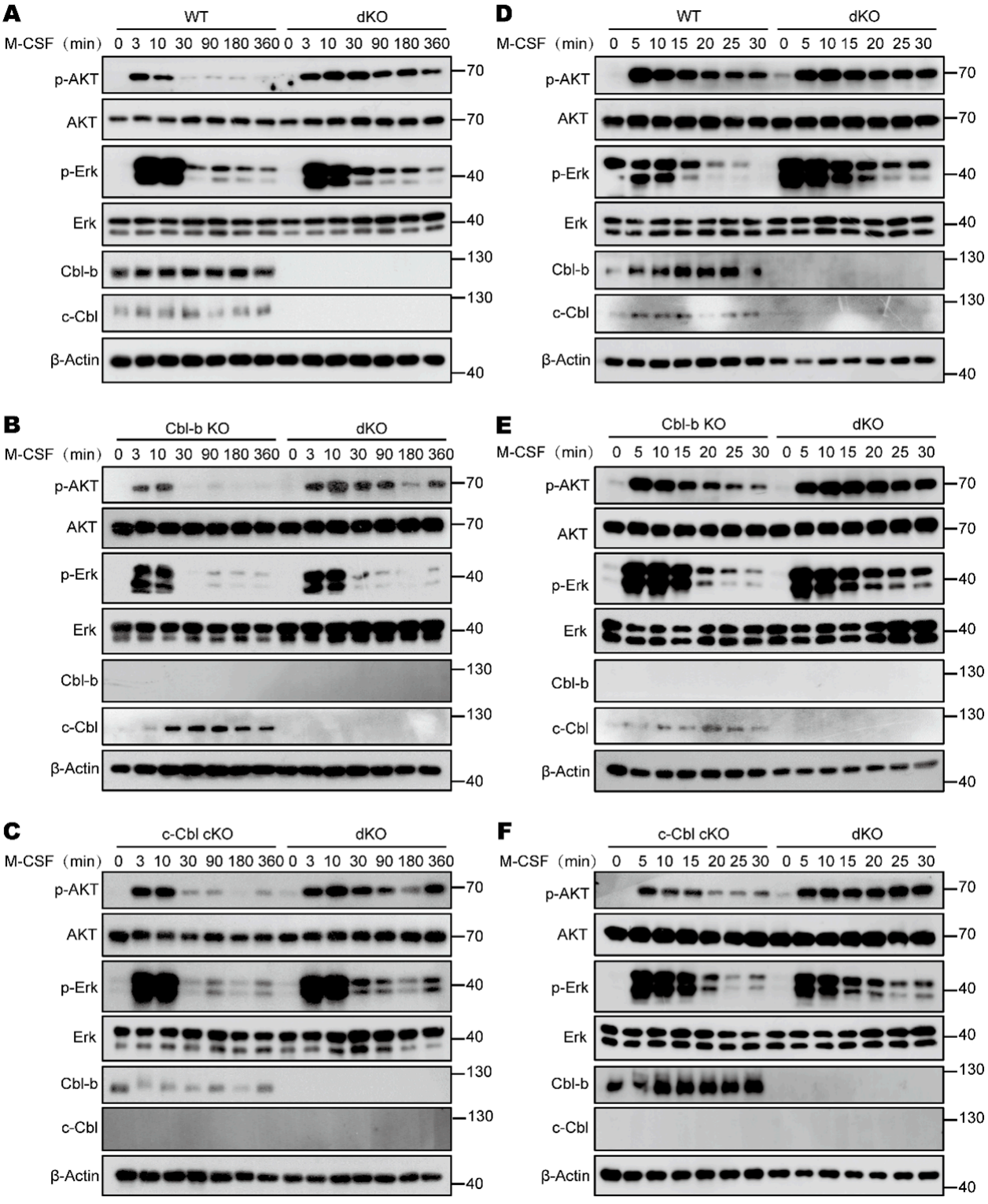

Figure 5

dKO BMDMs exhibit prolonged Akt and Erk activation upon M-CSF stimulation.

(**A and D**) WT and dKO BMDMs were starved of M-CSF for 24 h and restimulated with M-CSF (50 ng/mL) for indicated times and harvested for western blot analysis of p-AKT and p-Erk.

(**B and E**) Cbl-b KO and dKO BMDMs were starved of M-CSF for 24 h and restimulated with M-CSF (50 ng/mL) for indicated times and harvested for western blot analysis of p-AKT and p-Erk.

(**C and F**) c-Cbl cKO and dKO BMDMs were starved of M-CSF for 24 h and restimulated with M-CSF (50 ng/mL) for indicated times and harvested for western blot analysis of p-AKT and p-Erk.

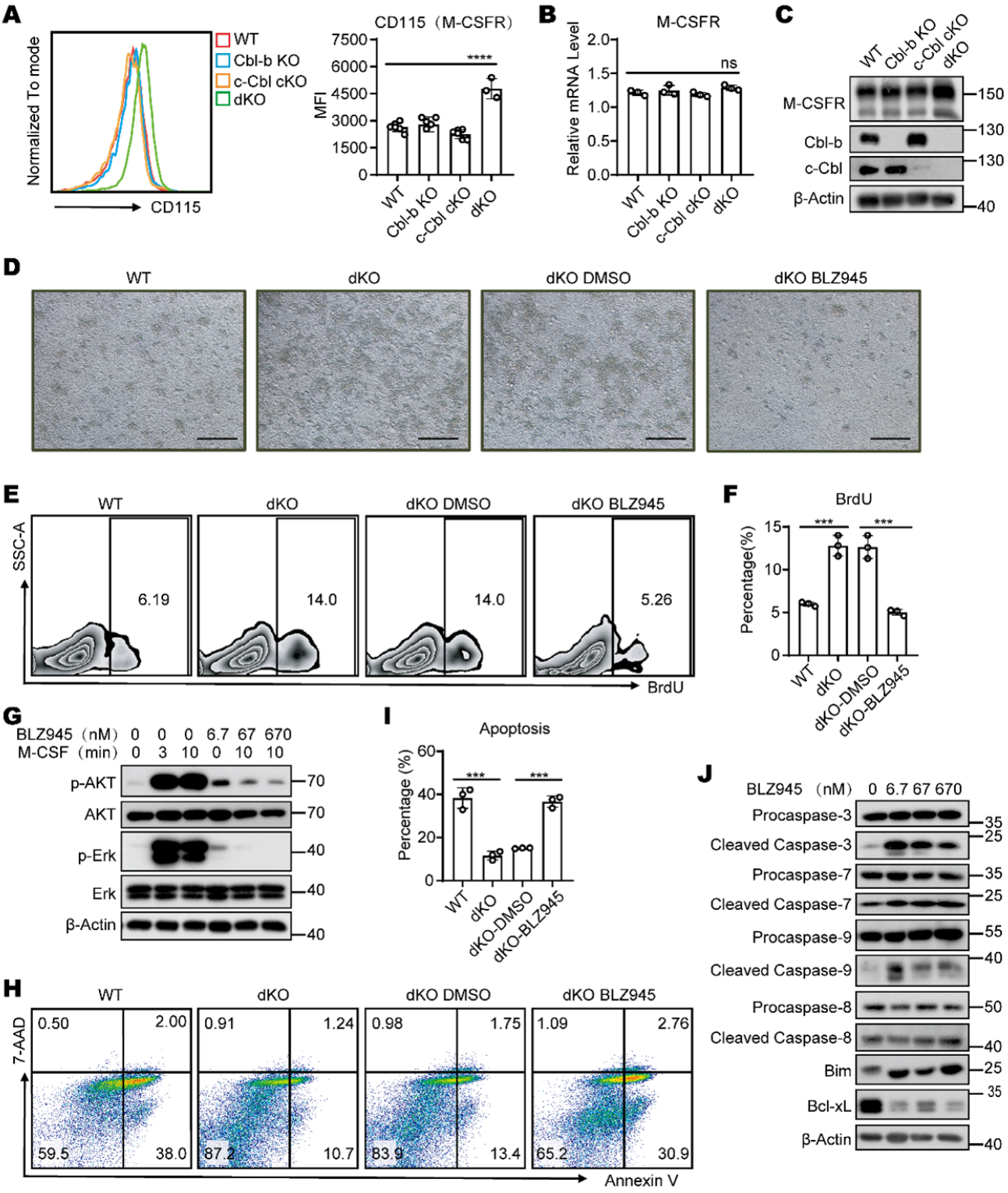

Figure 6

Cbl-b and c-Cbl collaboratively inhibit M-CSF-dependent cell proliferation and promote cell apoptosis by down-regulating M-CSFR protein levels.

(**A**) Flow cytometry analysis of cell surface expression of CD115 (M-CSFR) in WT, Cbl-b KO, c-Cbl cKO and dKO BALF AMs. *n* = 3-5 per group

(**B**) QPCR analysis of M-CFSR mRNA levels in WT, Cbl-b KO, c-Cbl cKO and dKO AMs.

(**C**) Western blot analysis of M-CSFR expression in WT, Cbl-b KO, c-Cbl cKO and dKO BMDMs.

(**D**) Microscopy of clonal morphology of four groups of mice macrophages induced by M-CSF; scale bar, 100 μm.

(**E and F**) Proliferation of WT and dKO BMDMs generated in M-CSF dependent BM cell culture which added BLZ945. Shown are FACS analyses (**E**) and statistics (**F**) of $BrdU^+$ $F4/80^+$ $CD11b^+$ cells. n = 3 per group.

(**G**) dKO BMDMs were starved of M-CSF for 24 h and treated with M-CSF (50 ng/mL) and different concentrations of BLZ945 for indicated times and harvested for western blot analysis of p-AKT and p-Erk.

(**H and I**) Apoptosis of WT and dKO BMDMs generated in M-CSF dependent BM cell culture which added BLZ945. Shown are FACS analyses (**H**) and statistics (**I**) of Annexin V^+ $7AAD^-$ and Annexin V^+ $7AAD^+$ $F4/80^+$ $CD11b^+$ cells. n = 3 per group.

(**J**) dKO BMDMs treated with different concentrations of BLZ945 and harvested for western blot analysis of cleaved caspase-3, -7, -8, -9, Bim and Bcl-xL. *ns*, no significance, **p*<0.05, ***p*<0.01, ****p*<0.001, *****p*<0.0001. *p*<0.05 was considered statistically significant.

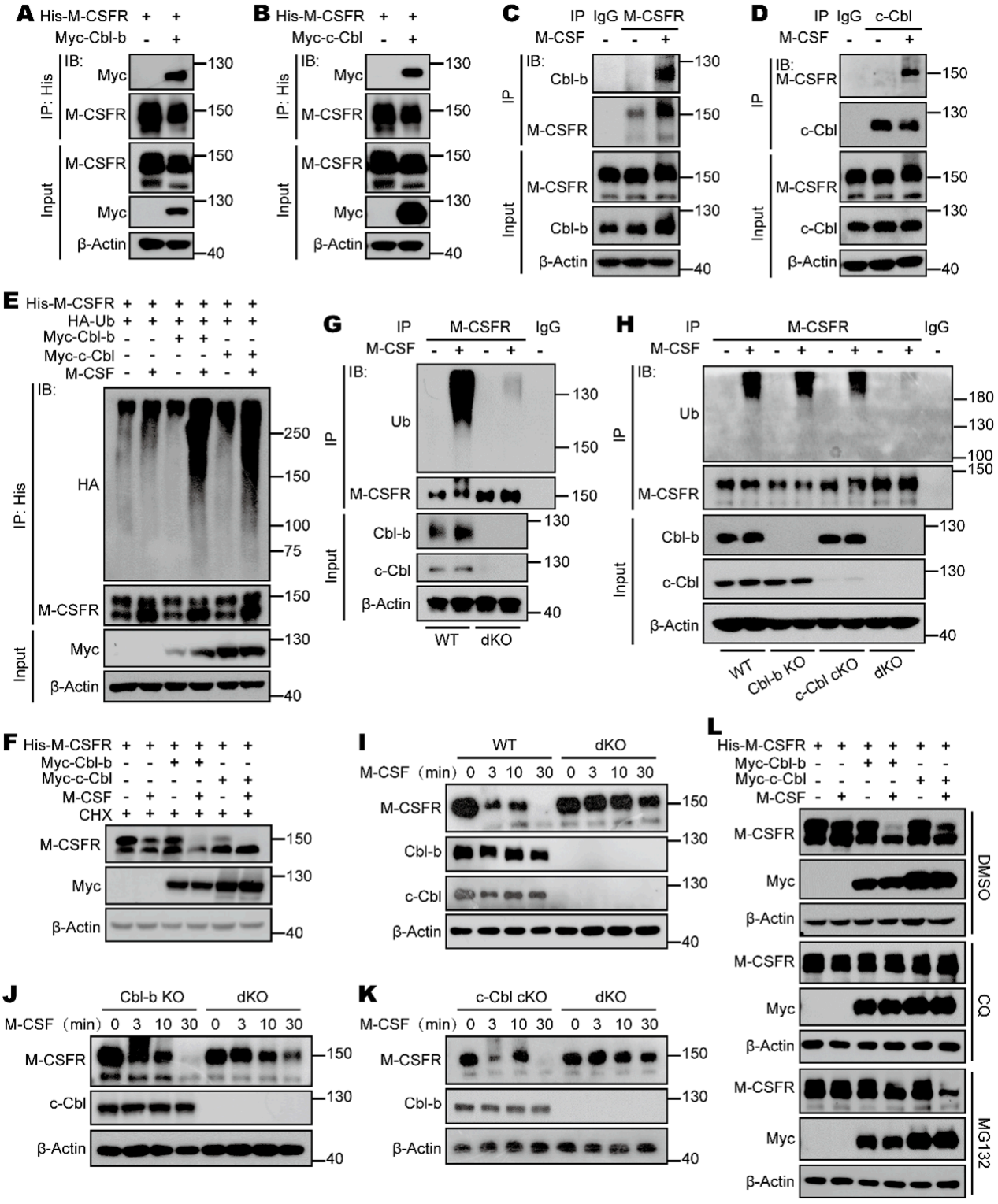

Figure 7

Cbls mediate M-CSF-induced the ubiquitination and degradation of M-CSFR.

(**A**) Immunoprecipitation analysis of the exogenous interaction between His-M-CSFR and Myc-Cbl-b in HEK293T cells.

(**B**) Immunoprecipitation analysis of the exogenous interaction between His-M-CSFR and Myc-c-Cbl in HEK293T cells.

(**C**) WT BMDMs were starved of M-CSF for 24 h and restimulated with M-CSF (50 ng/mL) and harvested for immunoprecipitation analysis of the endogenous interaction between M-CSFR and Cbl-b.

(**D**) WT BMDMs were starved of M-CSF for 24 h and restimulated with M-CSF (50 ng/mL) and harvested for immunoprecipitation analysis of the endogenous interaction between M-CSFR and c-Cbl.

(**E**) Immunoprecipitation analysis of polyubiquitination of M-CSFR in HEK293T cells cotransfected with His-M-CSFR, HA-Ub and Myc-Cbl (Cbl-b or c-Cbl) and then treated with M-CSF (50 ng/mL) for 2 h.

(**F**) Western blot analysis of M-CSFR in HEK293T cells cotransfected with His-M-CSFR and Myc-Cbl (Cbl-b or c-Cbl) and then treated with M-CSF (50 ng/mL) and CHX (50 μM) for 2 h.

(**G**) WT and dKO BMDMs were starved of M-CSF for 24 h and restimulated with M-CSF (50 ng/mL) for 3 min and harvested for immunocoprecipitation analysis of polyubiquitination of M-CSFR.

(**H**) WT, Cbl-b KO, c-Cbl cKO and dKO BMDMs were starved of M-CSF for 24 h and restimulated with M-CSF (50 ng/mL) for 3 min and harvested for immunocoprecipitation analysis of polyubiquitination of M-CSFR.

(**I**) WT and dKO BMDMs were starved of M-CSF for 24 h and restimulated with M-CSF (50 ng/mL) for indicated times and harvested for western blot analysis of degradation of M-CSFR.

(**J**) Cbl-b KO and dKO BMDMs were starved of M-CSF for 24 h and restimulated with M-CSF (50 ng/mL) for indicated times and harvested for western blot analysis of degradation of M-CSFR.

(**K**) c-Cbl cKO and dKO BMDMs were starved of M-CSF for 24 h and restimulated with M-CSF (50 ng/mL) for indicated times and harvested for western blot analysis of degradation of M-CSFR.

(**L**) Western blot analysis of M-CSFR in HEK293T cells cotransfected with His-M-CSFR and Myc-Cbl (Cbl-b or c-Cbl) and then treated with M-CSF (50 ng/mL), DMSO, CQ (20 μM) and MG132 (10 μM) for 2 h as indicated.

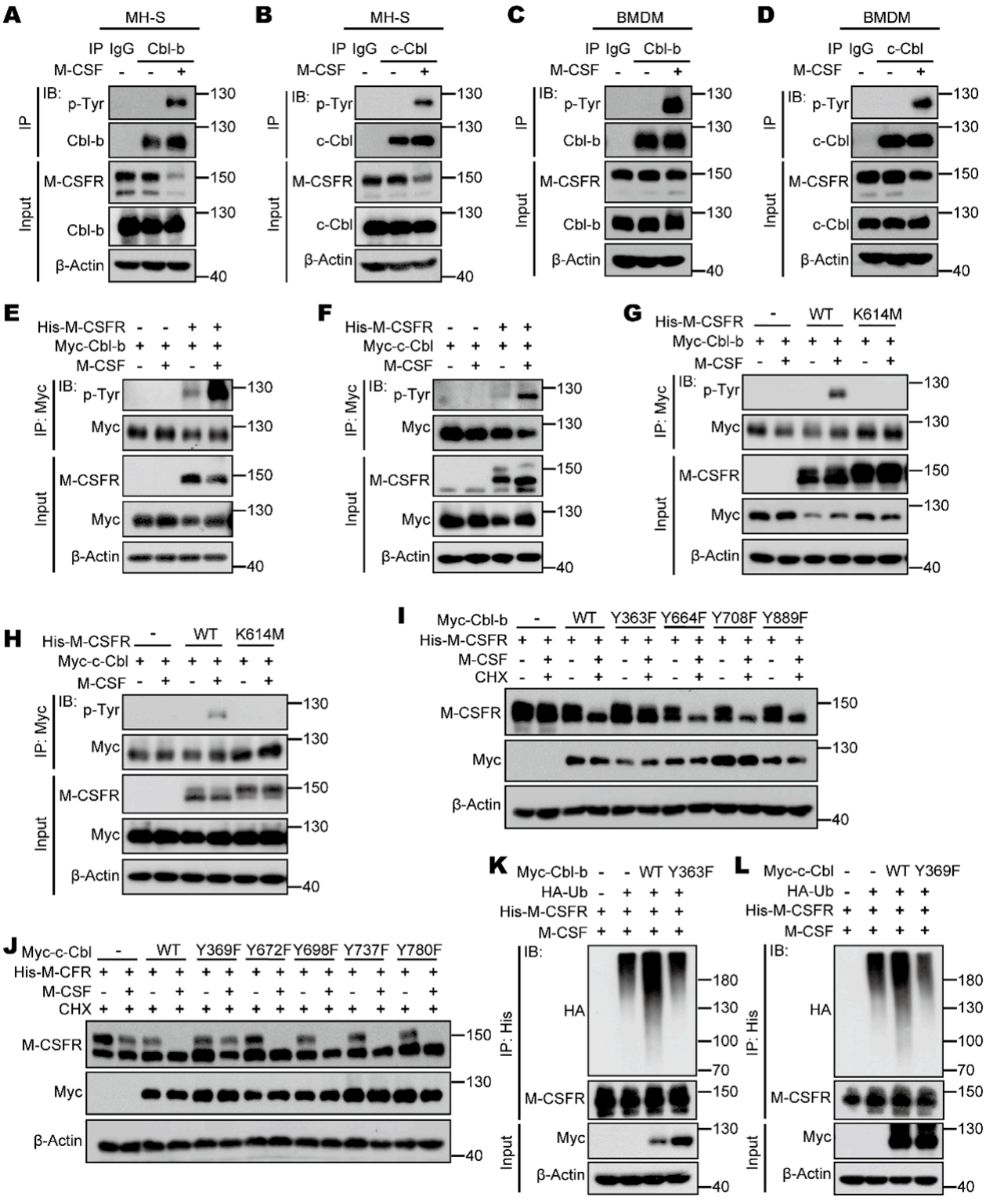

Figure 8

Phosphorylation of Cbls is critical for M-CSFR ubiquitination and degradation.

(**A**) Immunoprecipitation analysis of tyrosine phosphorylation of Cbl-b in RAW 264.7 cells treated with M-CSF (50 ng/mL).

(**B**) Immunoprecipitation analysis of tyrosine phosphorylation of c-Cbl in RAW 264.7 cells treated with M-CSF (50 ng/mL).

(**C**) WT BMDMs were starved of M-CSF for 24 h and restimulated with M-CSF (50 ng/mL) and harvested for Immunoprecipitation analysis of tyrosine phosphorylation of Cbl-b.

(**D**) WT BMDMs were starved of M-CSF for 24 h and restimulated with M-CSF (50 ng/mL) and harvested for Immunoprecipitation analysis of tyrosine phosphorylation of c-Cbl.

(**E**) Immunoprecipitation analysis of tyrosine phosphorylation of Cbl-b in HEK293T cells cotransfected with Myc-Cbl-b and His-M-CSFR and then treated with M-CSF (50 ng/mL) for 3 min.

(**F**) Immunoprecipitation analysis of tyrosine phosphorylation of c-Cbl in HEK293T cells cotransfected with Myc-c-Cbl and His-M-CSFR and then treated with M-CSF (50 ng/mL) for 3 min.

(**G**) Immunoprecipitation analysis of tyrosine phosphorylation of Cbl-b in HEK293T cells cotransfected with Myc-Cbl-b and His-M-CSFR (WT or K614M) and then treated with M-CSF (50 ng/mL) for 3 min.

(**H**) Immunoprecipitation analysis of tyrosine phosphorylation of c-Cbl in HEK293T cells cotransfected with Myc-c-Cbl and His-M-CSFR (WT or K614M) and then treated with M-CSF (50 ng/mL) for 3 min.

(**I**) Western blot analysis of M-CSFR in HEK293T cells cotransfected with His-M-CSFR and Myc-Cbl-b (WT or its tyrosine mutants) and then treated with M-CSF (50 ng/mL) and CHX (50 μM) for 2 h.

(**J**) Western blot analysis of M-CSFR in HEK293T cells cotransfected with His-M-CSFR and Myc-c-Cbl (WT or its tyrosine mutants) and then treated with M-CSF (50 ng/mL) and CHX (50 μM) for 2 h.

(**K**) Immunoprecipitation analysis of polyubiquitination of M-CSFR in HEK293T cells cotransfected with His-M-CSFR, HA-Ub and Myc-Cbl-b (WT or Y363F) and then treated with M-CSF (50 ng/mL) for 2 h.

(**L**) Immunoprecipitation analysis of polyubiquitination of M-CSFR in HEK293T cells cotransfected with His-M-CSFR, HA-Ub and Myc-c-Cbl (WT or Y369F) and then treated with M-CSF (50 ng/mL) for 2 h.

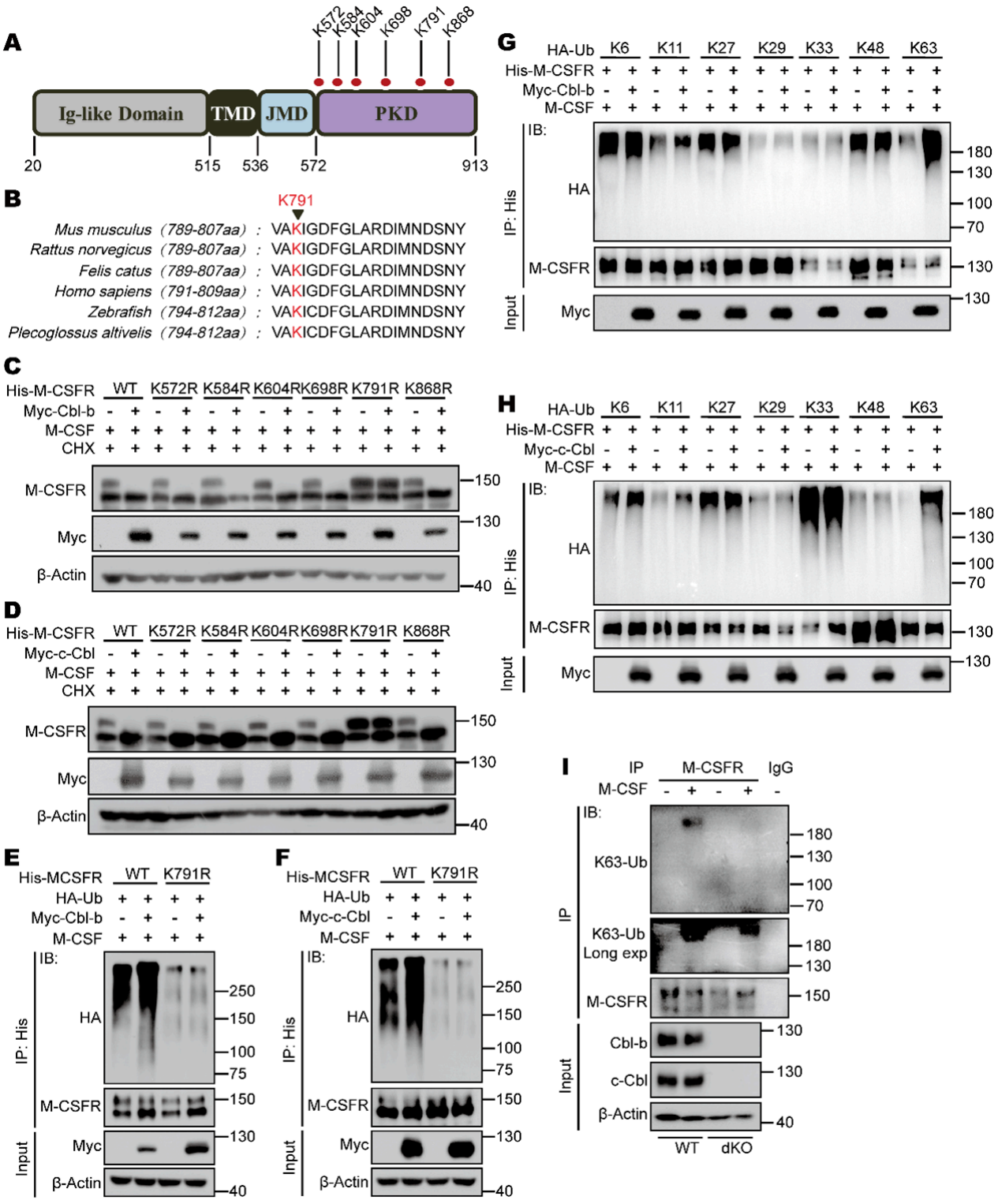

Figure 9

Cbls mediate the K63-linked polyubiquitination modification at Lys791 of M-CSFR.

(**A**) Model diagram of M-CSFR structure and its potential ubiquitination site.

(**B**) Highly conserved lysine (K) residues (K791) on M-CSFR from different species.

(**C**) Western blot analysis of M-CSFR in HEK293T cells cotransfected with His-M-CSFR (WT or its lysine mutants) and Myc-Cbl-b and then treated with M-CSF (50 ng/mL) and CHX (50 μM) for 2 h.

(**D**) Western blot analysis of M-CSFR in HEK293T cells cotransfected with His-M-CSFR (WT or its lysine mutants) and Myc-c-Cbl and then treated with M-CSF (50 ng/mL) and CHX (50 μM) for 2 h.

(**E**) Immunoprecipitation analysis of polyubiquitination of M-CSFR in HEK293T cells cotransfected with His-M-CSFR (WT or K791R), HA-Ub and Myc-Cbl-b and then treated with M-CSF (50 ng/mL) for 2 h.

(**F**) Immunoprecipitation analysis of polyubiquitination of M-CSFR in HEK293T cells cotransfected with His-M-CSFR (WT or K791R), HA-Ub and Myc-c-Cbl and then treated with M-CSF (50 ng/mL) for 2 h.

(**G**) Immunoprecipitation analysis of polyubiquitination types of M-CSFR in HEK293T cells cotransfected with His-M-CSFR, Myc-Cbl-b and different types of HA-Ub and then treated with M-CSF (50 ng/mL) for 2 h.

(**H**) Immunoprecipitation analysis of polyubiquitination types of M-CSFR in HEK293T cells cotransfected with His-M-CSFR, Myc-c-Cbl and different types of HA-Ub and then treated with M-CSF (50 ng/mL) for 2 h.

(**I**) WT and dKO BMDMs were starved of M-CSF for 24 h and restimulated with M-CSF (50 ng/mL) for 3 min and harvested for immunocoprecipitation analysis of K63-linked polyubiquitination of M-CSFR.

Supplementary Files

This is a list of supplementary files associated with this preprint. Click to download.

- SupplementalMaterial.docx